Cytokinin oxidase/dehydrogenase inhibitors: progress towards agricultural practice

Jaroslav Nisler, Pavel Klimeš, Radka Končitíková, Alena Kadlecová, Jiří Voller, Mahfam Chalaki, Michael Karampelias, Nino Murvanidze, Stefaan P O Werbrouck, David Kopečný, et al.

Cytokinin oxidase/dehydrogenase inhibitors: progress towards agricultural practice

Jaroslav Nisler[1,*], Pavel Klimeš[2], Radka Končitíková[3], Alena Kadlecová[3], Jiří Voller[3], Mahfam Chalaki[1,4], Michael Karampelias[5], Nino Murvanidze[6], Stefaan P.O. Werbrouck[6], David Kopečný[3], Libor Havlíček[1], Nuria de Diego[2], Pierre Briozzo[7], Solange Moréra[8], David Zalabák[9], Lukáš Spíchal[2]

[1]*Isotope Laboratory, Institute of Experimental Botany, The Czech Academy of Sciences, Vídeňská 1083, 142 20 Prague, Czech Republic.*

[2]*Czech Advanced Technology and Research Institute (CATRIN), Palacký University Olomouc, Šlechtitelů 27, Olomouc CZ-783 71, Czech Republic*

[3]*Department of Experimental Biology, Faculty of Science, Palacký University, Šlechtitelů 27, Olomouc CZ-78371, Czech Republic*

[4]*Department of Experimental Plant Biology, Faculty of Science, Charles University, Viničná 5, CZ-128 43 Prague 2, Czech Republic*

[5]*Laboratory of Hormonal Regulations in Plants, Institute of Experimental Botany of the Czech Academy of Sciences, Rozvojová 263, 165 02 Praha 6, Czech Republic*

[6]*Department Plants and Crops, Faculty of Bioscience Engineering, Ghent University, Ghent, Belgium*

[7]*Institut Jean-Pierre Bourgin, INRAE, AgroParisTech, Université Paris-Saclay, Route de Saint-Cyr, F-78026, Versailles, France*

[8]*Institute for Integrative Biology of the Cell (I2BC), CEA, CNRS, Université Paris-Saclay, 91198, Gif-sur-Yvette, France*

[9]*Laboratory of Growth Regulators, Institute of Experimental Botany of the Czech Academy of Sciences & Palacký University, Šlechtitelů 27, CZ-783 71 Olomouc, Czech Republic*

* Correspondence: Jaroslav Nisler; Email: jaroslav.nisler@gmail.com;

Tel.: +420 608 122 530

E-mail address for each author:

Jaroslav Nisler: jaroslav.nisler@gmail.com

Pavel Klimeš: pavel.klimes@upol.cz

Radka Končitíková: radka.koncitikova@gmail.com

Alena Kadlecová: alena.kadlecova@upol.cz

Jiří Voller: jirivoller@gmail.com

Mahfam Chalaki: mahfam995chalaki@gmail.com

Michael Karampelias: karampelias@ueb.cas.cz

Nino Murvanidze: nina.murvanidze@gmail.com

Stefaan P.O. Werbrouck: Stefaan.Werbrouck@ugent.be

David Kopečný: david.kopecny@upol.cz

Libor Havlíček: lihavlic@biomed.cas.cz

Nuria de Diego: nuria.de@upol.cz

Pierre Briozzo: pierre.briozzo@inrae.fr

Solange Moréra: solange.morera@i2bc.paris-saclay.fr

David Zalabák: david.zalabak@upol.cz

Lukáš Spíchal: lukas.spichal@upol.cz

Highlight

This structure-activity relationship study of a new series of cytokinin oxidase/dehydrogenase inhibitors demonstrates compounds with very high efficacy, low toxicity, and high practical potential for agricultural use.

Abstract

Cytokinin oxidase/dehydrogenase (CKX) inhibitors reduce the degradation of cytokinins in plants and thereby may improve the efficiency of agriculture and plant tissue culture-based practices. Here, we report a synthesis and structure-activity relationship study of novel urea derivatives concerning their CKX inhibitory activity. The best compounds showed sub-nanomolar IC_{50} values with maize ZmCKX1, the lowest value yet documented. Other CKX isoforms of maize (*Zea mays*) and Arabidopsis were also inhibited very effectively. The binding mode of four compounds was characterized based on high-resolution crystal complex structures. Using the soil nematode *Caenorhabditis elegans*, and human skin fibroblasts, key CKX inhibitors with low toxicity were identified. These compounds enhanced the shoot regeneration of *Lobelia*, *Drosera*, and *Plectranthus*, as well as the growth of Arabidopsis and *Brassica napus*. At the same time, a key compound (namely **82**), activated a cytokinin primary response gene *ARR5:GUS* and cytokinin sensor *TCSv2:GUS*, without activating the Arabidopsis cytokinin receptors AHK3 and AHK4. This strongly implies that the effect of compound **82** is due to the upregulation of cytokinin signalling. Overall, this work presents highly effective and easily prepared CKX inhibitors with a low risk of environmental toxicity for further investigation of their potential in agriculture and biotechnology.

Keywords: agriculture, biostimulant, biotechnology, CKX inhibitor, cytokinin, cytokinin oxidase/dehydrogenase, diphenylurea, nutrient use efficiency, oilseed rape, Arabidopsis

Abbreviations: CKX – cytokinin oxidase/dehydrogenase, DCPIP – 2,6-dichlorophenolindophenol; DPU – diphenylurea, IC_{50} – half-maximal inhibitory concentration; iP – N^6-isopentenyladenine; MTT – 3-(4,5-dimethylthiazol-2-yl)-2,5-diphenyltetrazolium bromide, PMS – phenazine methosulfate, TFM – trifluoromethoxy (group).

Introduction

Increasing the efficiency of agricultural practices is in constant focus due to the ever-increasing demand for food production in a changing climate. Reducing the cost of inputs and the negative impact of new agrotechnologies on the environment is an integral part of this effort. One method of achieving these goals is the use of plant growth regulators, compounds that can regulate plant growth and development.

One such group of compounds are plant hormones, the cytokinins, which regulate essential plant processes such as cell division in meristems, growth of shoots, leaves, roots, and reproductive organs, and senescence; amongst other effects (Kieber and Schaller, 2014). In plants, cytokinins are degraded by cytokinin oxidase/dehydrogenase (CKO/CKX, EC 1.5.99.12, Chatfield and Armstrong, 1986; Hare and Van Staden, 1994), which catalyzes their irreversible oxidative degradation, thereby reducing their levels. CKX proteins are encoded by a gene family and the individual enzyme isoforms usually differ in substrate specificity, spatial and temporal expression patterns, and subcellular localization (e.g. Šmehilová *et al*., 2009; Vyroubalová *et al*., 2009). For example, *Zea mays* contains 13 *CKX* genes, of which *ZmCKX1* plays a crucial role in cytokinin degradation (Houba-Hérin *et al*., 1999; Morris *et al*., 1999). *Arabidopsis thaliana* has seven CKXs (Werner *et al*., 2003), of which AtCKX2 is the most active and well-studied isoform (Galuszka *et al*., 2007).

It was previously shown that protecting cytokinins from their degradation can significantly improve plant stress tolerance, growth, and yield. Examples were provided with the use of genetically modified plants with reduced *CKX* expression (Ashikari *et al*., 2005; Zalewski *et al*., 2010; Bartrina *et al*., 2011; reviewed by Chen *et al*., 2020), as well as with CKX inhibitors that inhibit the CKX function (Gemrotová *et al*., 2013; Aremu *et al*., 2014; Camblin and Pingel, 2017; Camblin *et al*., 2017; Kon *et al*., 2017; Nisler *et al*., 2021). However, if CKX inhibitors are to find application in practice, these compounds must meet several other criteria, in addition to demonstrating efficacy.

First, their use must be economically beneficial. This means that the chemicals used for synthesis need to be simple and readily available commercially at a reasonable price. The synthetic process should also be simple and consist of a minimum number of steps to get closer to the concept of green chemistry. Only then, can the production of such chemicals (plant growth regulators) be of interest to agrochemical companies, and a product has a chance to enter the market. Second, the application of CKX inhibitors should not pose a risk to humans and the environment.

In our recent works (Nisler *et al*., 2021 and 2022), we have described the design, synthesis, and range of biological activities of 68 CKX inhibitors. The key compounds presented in the first work contain a hydroxyalkyl group, which has to be protected by some protecting group during synthesis and the same group must be removed at the end. These steps complicate both the synthesis and the subsequent isolation of the product. In the second work, we presented compounds with simple structure and synthesis, but the most active compounds exhibited high toxicity against the nematode *Caenorhabditis elegans* and against bacteria and human cell lines (De Resende *et al*., 2023).

In this work, we present CKX inhibitors in which the role of the hydroxyalkyl group has been taken over by an amide group, and whose synthesis is simpler. Using X-ray crystallography, we show what role the amide group plays and what interactions with ZmCKX4a and ZmCKX8 forms. Furthermore, we show that this amide group enhances the inhibitory properties of urea-derived CKX inhibitors against key CKX isoforms from maize and Arabidopsis. The key compounds described herein were further tested for use in biotechnology such as plant tissue culture and as potential biostimulants for agriculture.

Material and methods

Cytokinins and chemicals

2-Aminobenzamide, 3-chloro-5-methylaniline, 3-chloro-5-(trifluoro-methoxy)aniline, 2-amino-4-chlorobenzoic acid, 2-amino-4-bromobenzoic acid, 2-amino-4-methoxybenzoic acid and 2-amino-4-(trifluoromethoxy)benzonitrile were from Fluorochem, UK (http://www.fluorochem.co.uk/). 2-Amino-4,6-dichlorobenzoic acid, (2-amino-4-chlorophenyl)methanol, and 3-chloro-5-fluoroaniline were from Activate scientific, UK (www.activate-scientific.com). 2-(2-Aminophenyl)ethan-1-ol, 3,5-diflouroaniline, 1,3-dichloro-5-isocyanatobenzene, 1-chloro-3-isocyanatobenzene, tert-butylchlorodimethylsilane, 3-aminobenzamide methyl 2-amino-4-methoxybenzoate, ethylamine hydrobromide, 2-aminoethan-1-ol, ethane-1,2-diamine, hydrazine, 2-amino-N-hydroxybenzamide were from Sigma Aldrich, USA (https://www.sigmaaldrich.com). The cytokinin N^6-isopentenyladenine (iP) was from Olchemim, Czech Republic (https://www.olchemim.cz/). Other chemicals and solvents were purchased from usual commercial sources.

General synthesis

In our previous studies, we described 68 CKX inhibitors (Nisler *et al*., 2021; 2022), and the numbering of compounds here follows directly from that. Compounds **69–103** (Protocol S1) were synthesized by nucleophilic addition of aniline to isocyanatobenzene, all of which were substituted by corresponding substituents (halogens, methoxy group, trifluoromethoxy group, amide group, carboxylic acid group, etc.). If the isocyanatobenzene was not commercially available it was synthesized from aniline and diphosgene as described earlier (Nisler *et al*., 2021).

Another starting material was 2-aminobenzamide optionally substituted in position 4. These substituted 2-aminobenzamides were prepared from corresponding aromatic carboxylic acids by amidation reaction using 1-ethyl-3-(3-dimethylaminopropyl)carbodiimide HCl salt (Rebek and Feitler 1973) and hydroxybenzotriazole (Windridge and Jorgensen 1971). Details of syntheses and chemical-physical characterization of all intermediate compounds not previously described and the same data for all final products are presented in Protocol S1. The compounds were characterized by MS-ESI, ^{1}H NMR, and melting-point analysis according to Nisler *et al*. (2021).

General experimental procedures

Physico-chemical analyses, including HPLC purity, melting point (mp), Mass spectra, ^{1}H NMR spectra, and UV spectra were obtained as described in Nisler *et al*. 2021, 2022. ATR IR spectra were recorded on the Nicolet iS5 FT-IR Spectrometer with an iD7 ATR Accessory (both from Thermo Scientific, UK). The HPLC purity of compounds (%) was recorded at a compound absorption maximum (λ_{max}), and it had to be 97.0% or higher for the compound to be used in biological experiments.

CKX inhibition measurements

Pure enzymes were used in the case of ZmCKX1, ZmCKX4a, and ZmCKX8. ZmCKX1 was expressed in the yeast *Yarrowia lipolytica* and purified according to a published protocol (Kopečný *et al*., 2005). ZmCKX4a and ZmCKX8 were expressed in *Escherichia coli* BL21 STAR (DE3) cells carrying pTYB12-ZmCKX4a and ZmCKX8 plasmids, respectively. The enzymes were purified as previously described (Zalabák *et al*., 2014). AtCKX2 was produced into the growth media by *Saccharomyces cerevisiae* and used according to Frébortová *et al*. (2007).

The ability of the synthesized compounds to inhibit CKXs was determined based on their IC_{50} values obtained in the CKX inhibition assay. In this study, the CKX inhibition assay was conducted using two distinct methods, both described by Frébort *et al*. (2002). For AtCKX2 and ZmCKX1, the electron acceptor 2,6-dichlorophenolindophenol (DCPIP) was employed. In the case of ZmCKX4a and ZmCKX8 a mixture of phenazine methosulfate and 3-(4,5-dimethylthiazol-2-yl)-2,5-diphenyltetrazolium bromide (PMS/MTT) was used. In our previous work, we reported the IC_{50} values of compound **19** (Nisler et al., 2021, Table 2) with AtCKX2, ZmCKX1, ZmCKX4a and ZmCKX8 using DCPIP. Later, in Nisler et al. (2022) we reported the IC_{50} values of compound **52** using DCPIP with AtCKX2 and ZmCKX1, and PMS/MTT with ZmCKX4a. For ZmCKX4a and ZmCKX8, we started using the MPS/MTT method because it repeatedly provided more accurate and more reproducible results.

All pipetting steps were performed using an Opentrons II liquid handling station (Opentrons, USA), and enzyme inhibition was measured in a 384-well plate. Details of the procedure were described by Nisler *et al*. (2022). Briefly, the tested compounds were first automatically diluted in 100% DMSO to concentrations of 10 mM, 1 mM, 100 µM, 10 µM, 1 µM, 100 nM, and 10 nM, respectively. Subsequently, the inhibition assay was performed in a reaction mixture consisting of potassium phosphate buffer (100 mM, pH 7.4), EDTA (2.1 mM), BSA (2.1 mg ml^{-1}), and 0.2 mM DCPIP or a mixture of PMS/MTT (0.2 mM PMS, 1 mM MTT). In all reactions, iP at a saturating concentration (45 µM for AtCKX2 and ZmCKX4a, 10 µM for ZmCKX1, and 12 µM for ZmCKX8) was used as substrate. Finally, the enzyme (50 pkat ml^{-1} for AtCKX2, 20 pkat ml^{-1} for ZmCKX1, 50 pkat ml^{-1} for ZmCKX4a and ZmCKX8) was added to the mixture. In blank samples, the substrate and tested compounds were replaced by DMSO in the reaction mixture. The compounds were tested in at least two replicates, and the entire test was repeated at least twice. The BioTek™ Synergy™ H4 reader (USA) was used for the incubation of the well plate at 37 °C and the acquisition of kinetic data every 2 minutes for 20 minutes at 590 nm (2,6-dichlorophenolindophenol assay) or 578 nm (PMS/MTT assay). For each compound, a concentration-dependent curve of CKX residual activity was constructed, and the IC_{50} value was determined using Python script.

Crystallization and structure determination

Crystals were obtained in hanging drops upon co-crystallization of ZmCKX4a and ZmCKX8 with various tested inhibitors. ZmCKX8 (12 mg/ml) was co-crystallized in 0.1 M HEPES buffer (pH 7.5) with 27% polyethylene glycol 4000, and 4 mM inhibitor (compound **71**) in

the final drop. In the case of compound **77**, the condition consisted of 50 mM Tris-HCl buffer pH 8.0, 15% polyethylene glycol 1500, and 1.5 mM inhibitor. Crystals were cryoprotected with the mother liquor supplemented with 20% glycerol and flash-frozen in liquid nitrogen. ZmCKX4a was co-crystallized with four inhibitors in 0.1 M HEPES (pH 7.5) containing 35-40% 2-methyl-2,4-pentanediol and 1-5 mM inhibitor. Due to the presence of 2-methyl-2,4-pentanediol, the crystals were directly flash-frozen in liquid nitrogen.

Datasets of ZmCKX4 and ZmCKX8 complexes were collected at 100 K on the Proxima 1/2 beamlines of the SOLEIL synchrotron (www.synchrotron-soleil.fr). Diffraction intensities were integrated with the program XDS (Kabsch, 1993), and all structures were solved by molecular replacement with Phaser (McCoy *et al*., 2007). The data quality of the datasets was assessed using the correlation coefficient CC1/2 (Karplus and Diederichs, 2012). Models were refined using Buster 2.10 (Bricogne *et al*., 2011) to a resolution of 1.8 Å and ligand occupancies set to 1. Electron density maps were evaluated using Coot (Emsley and Cowtan, 2004). Data collection and refinement statistics are given in Table S1. The model quality was assessed with MolProbity (Chen *et al*., 2010). Graphical images were generated with PYMOL 2.5 (https://pymol.org/). The atomic coordinates and structure factors have been deposited in the Protein Data Bank (www.wwpdb.org). Two ZmCKX8 inhibitor complexes with compounds **71** and **77** have accession codes 8CJ9 and 8CK6, respectively. Four ZmCKX4a inhibitor complexes with compounds **71**, **77**, **78**, and **99** have been deposited under the accession codes 8CKQ, 8CLW, 8CKT, and 8CM2, respectively. Ligand interactions were further analyzed using Discovery Studio Visualizer v.21.1.0. (BIOVIA, San Diego, USA).

Toxicity evaluation in Caenorhabditis elegans

The wild-type N2 (Bristol) strain of *Caenorhabditis elegans* and the *Escherichia coli* bacteria strain OP50 were used in this study. Compounds **69–103** were tested for their toxicity based on their effects on the fecundity of *C. elegans* exactly as described by Nisler *et al*. (2022). The experiment was performed three times, in two replicates for each treatment.

Toxicity evaluation in BJ cells

The effect of 72-hour treatments with the test compounds on human BJ (skin fibroblasts) cell line viability was evaluated using a resazurin reduction assay, measuring the metabolic activity of the cell population. BJ cells were obtained from the American Type Culture

Collection, Manassas. The assay was carried out according to Voller *et al*. (2019). The experiment was repeated three times, in two replicates for each treatment.

Regeneration of shoots

Drosera rotundifolia, Lavandula angustifolia, Lobelia erinus, Plectranthus esculentum, and *Sempervivum tectorum* were selected from the ongoing *in vitro* collections. Leaf explants of an average of 0.5 cm^2 were cut and transferred to the shoot induction medium. This consisted of Murashige and Skoog (MS) medium, 30 g/l sucrose, 7 g/l agar, and 1 µM iP. The pH of the media was adjusted to 5.8 before autoclaving. Compounds **19** and **77** were added into the medium after autoclaving at a concentration of 1 µM. The cultures were incubated at ± 22 ºC, at a 16 h light/8 h dark photoperiod. The experiment was performed once in two independent replicates, each with ten explants for each treatment. Data were evaluated after a five-week incubation period.

Cytokinin receptor activation and competitive assays

E. coli strain KMI001, harboring either the plasmid pIN-IIIAHK4 or pSTV28-AHK3, which express the Arabidopsis histidine kinases CRE1/AHK4 (hereafter as AHK4 only) or AHK3 (Suzuki *et al.,* 2001; Yamada *et al.*, 2001) was used in 1) cytokinin receptor activation assay, performed as previously described Spíchal *et al.* (2004); and 2) live-cell hormone-binding assay, performed generally as described Romanov *et al.* (2005) with minor modifications (Nisler *et al.,* 2010). Cytokinin receptor activation assays were performed once, in triplicates for each treatment. Cytokinin receptor competitive assays were performed twice, in duplicates for each treatment.

Arabidopsis ARR5:GUS and TCSv2:GUS reporter gene assay

Arabidopsis ARR5:GUS transgenic plants were used in this assay described previously (Romanov *et al.,* 2002). Quantitative determination of GUS activity in plants was performed after 16 hours of exposure to the test compounds by measuring fluorescence with minor modifications (Nisler *et al.,* 2010). The entire test was performed twice, in triplicates for each treatment. Histochemical analysis of *beta*-glucuronidase (GUS) activity in seedlings expressing the *TCSv2:GUS* (*TWO-COMPONENT OUTPUT SENSOR VERSION2,* Steiner et al., 2020) was performed using a GUS staining buffer with 1mg/ml X-Gluc (Jefferson et al., 1987). After 6 days of germination in half-strength MS medium with 10% sucrose and 1% plant agar, Arabidopsis seedlings were transferred to liquid, half-strength MS medium

containing 1 μM compound **82** or 1 μM *trans*-zeatin and plants for 48 hours. From 12 to 15 seedlings were used for each treatment, and we used 4 to 6 to take photos in a dissecting widefield microscope (Zeiss AxioImager Z2) with a 5x objective lens.

Plant material and growing conditions of Arabidopsis

Seeds of *Arabidopsis thaliana* (L.) Heynh. (Col-0 ecotype) were surface sterilized with 70% ethanol plus 0.01% Triton X-100 following the protocol described by De Diego *et al*. (2017). Then seeds were distributed homogeneously with the help of toothpicks autoclaved on a sheet of autoclaved filter paper moistened with sterile water under laminar flux chamber conditions. After 4 min, the filter paper with the seeds was transferred to a square plate (120 × 120 mm, P-Lab, Ref. 212358.2) containing half-strength solid MS medium (Phytotechlab M519) with the four testing compounds (**81**, **82**, **77** or **19**) at four different concentrations (0.01, 0,1, 1 or 10 μM), or without compound as a negative control, as described by Ugena *et al*. (2018). After sowing, the square plates were kept in the dark at 4 °C for 4 days, followed by an additional 4 days located vertically in the growth chamber under controlled conditions with a photoperiod 16/8 h (light/dark) with a light intensity of 120 μmol photons s^{-1} m^{-2}, a temperature of 22 °C, and a relative humidity of 60%. Afterwards, the Arabidopsis seedlings were transferred to 48-well plates filled with 1×MS growth medium for control conditions or 1/3×MS for low nutrition. All media were adjusted to pH 5.7 and supplemented with 0.6% Phytagel. The plates were placed in the OloPhen platform that uses the PlantScreen™ XYZ system installed in a growth chamber with a controlled environment (De Diego *et al*. 2017). The growth conditions were set to simulate a long day with a regime of 22/20 °C in a 16/8 h light/dark cycle, an irradiance of 120 μmol photons of PAR m^{-2} $s^{-1,}$ and a relative humidity of 60%.

Non-invasive multi-trait high-throughput screening of Arabidopsis rosette growth

Once the plates were placed in the phenotyping system, they were photographed using a red-green-blue camera twice daily for 7 days, as described by Ugena *et al*. (2018). Several features were extracted from the image analysis; early seedling establishment (green pixels), which describes the size of the seedlings on the first day they were placed in the system and defines the effect of the compound pre-treatment on the seedling size; the final area and perimeter of the seedlings on the last day of measurement, the absolute and relative growth rate, three indexes describing the greenness of the plants (Ugena *et al*., 2018), and the

standard deviation of the final area as a parameter to define the homogeneity of the population. The data were displayed in a parallel coordinate plot.

Experiment with oilseed rape

Seeds of winter oilseed rape (*Brassica napus* var. aganos) were sown on wet cotton tissue. Two days after germination, the selected seeds were transferred to larger pots (upper diameter 20 cm) filled with expanded clay (keramzite, diameter 4-8 mm) and full-nutrient solution (Krystalon, Yaaragri, CZ; 4g/l) with or without the addition of compounds **77** and **82** at 100 nM concentration. Each pot contained 3 plants. Four pots (12 plants) were used for each variant. Plants were watered regularly with tap water to equal weight. The pots were placed in a growth chamber with a 14/10 (light/dark) photoperiod, a light intensity of 500 µmol photons m^{-2} s^{-1}, 60% humidity, and a temperature of 18–24°C. The experiment was terminated 20 days after germination when the fresh weight of roots and shoots was determined.

Results

Design and chemistry of novel CKX inhibitors

In our two previous studies, we described 68 CKX inhibitors derived mainly from diphenylurea (DPU) (Nisler *et al*., 2021; 2022). Here we designed, synthesized, and tested another 34 CKX inhibitors, numbered **69–103**. The chemical structures of new compounds were proposed gradually, always based on testing (IC_{50}) of previously prepared compounds with the ZmCKX1. Initially, compound **71** was prepared as part of a previously published series of compounds **6–15** (Nisler *et al*., 2021). However, the IC_{50} of compound **71** with ZmCKX1 was unusually low, deviating from the IC_{50}s of other compounds in the group (Nisler *et al*., 2021; Fig. S1). To analyze whether the amide group of **71** interacts with the active site of ZmCKX1 in the same cavity as the hydroxyethyl group of **19** (3TFM-2HE) (Fig. 1A), compound **73** was prepared. The IC_{50} of **73** (with ZmCKX1) was higher than that of compound **71** (Table 1; Fig. S1) which indicated that the amide group did not fit in the presumed location. Therefore, we speculated that compound **71** flipped (Fig. S1) and its amide group has interacted with the active site of ZmCKX1 at the location adjacent to positions 2´ and 3´ of the 3TFM-2HE molecule, which also contains several polar residues (Fig. 1A). Then, the IC_{50} of compound **78** provided clear evidence that our assumption was correct. This also meant that two chlorines (in positions 3 and 5) of compound **71** fit perfectly

into the internal cavity of the active site of ZmCKX1. This result is consistent with our previous findings (Nisler *et al*., 2022). Subsequently, compounds **69–84** were prepared to analyze the effect of various substituents in combination with the amide group (Fig. 1B). To examine the effect of the amide group modifications on CKX inhibitory activity compounds **85–94** were prepared (Fig. 1B). To analyze the effect of combining the hydroxyalkyl group in position 2 with the amide group in position 2´ compounds **95–99** were prepared (Fig. 1C). Compounds **100–103** were side products of the syntheses.

The vast majority of compounds **69–103** are new, previously undescribed chemicals. Thus, all final products were characterized by MS-ESI, ^{1}H NMR, and melting-point analysis (Protocol S1).

Inhibition of ZmCKX1

The IC_{50} values obtained with compounds **69–73** show that two chlorines on the phenyl ring not carrying the amide group are the best option for inhibition. When one of those chlorines is missing (compound **69**) the inhibitory strength is ~ 20-fold weaker. On the opposite, when one of those chlorines is substituted by fluorine, methyl, or trifluoromethoxy (TFM) group, the weakening of the inhibitory strength is much less profound (Table 1).

Importantly, when the amide group in position 2´ was combined with substituents in position 5´, which are known to enhance the CKX inhibition (Nisler *et al*., 2021, 2022), the CKX inhibitory strength was significantly improved (compounds **75–78**). Thus, these compounds whose IC_{50} reaches sub-nanomolar levels are the most potent ZmCKX1 inhibitors ever published. Interestingly, there is no significant difference between the IC_{50}s of these compounds that otherwise carry substituents of different strengths at the 5´ position. Notably, when the chlorine atom was also present in position 3´, the inhibitory effect was markedly decreased (compare the IC_{50} of compounds **74** and **75**). Regarding compounds **79–84**, omission of one or both chlorines, or replacement of one or both of the chlorines with a fluorine atom decreased the CKX inhibition, similarly as shown before with compounds **69** and **70**, and with compounds **53** and **54** from our previous work (Nisler *et al*., 2022).

Of compounds **85–94**, compounds **85** and **86** exhibited very low IC_{50} values (around 2 nM). This means the amide group can have *N*-substituents, such as ethyl or 2-hydroxyethyl, without losing its strong effect. Compounds **87** and **88**, with an *N*-(2-aminoethyl) and *N*-amino group, respectively, showed slightly lower activity. Compound **89**, with the *N*-

hydroxyl group, was about 40 times weaker than compound **71**. When the amide group was replaced by the carboxylic acid group (compounds **90–92**) or the methyl ester group (compound **93**) the inhibitory strength decreased by two orders of magnitude. When the amide group was introduced to the 3´ instead of the 2´ position, the inhibitory strength decreased 15 times (compare the IC_{50} of compounds **71** and **94**).

It has previously been shown that the hydroxyalkyl group in position 2 on DPU derivatives increases CKX inhibitory activity (Nisler *et al*., 2016, 2021, 2022). The comparison of the IC_{50} of compounds **95–99** with those of corresponding compounds without the 2-hydroxyethyl group provides us with an important piece of information. There is no additive or synergistic effect of the amide and the hydroxyalkyl group on ZmCKX1 inhibition (compare the IC_{50} of compounds **97** and **98** with that of **82**, and the IC_{50} of compound **99** with that of **78**). On the contrary, the presence of both groups seems to complicate the inhibition slightly.

Another interesting result was obtained with compound **101** which has six substituents, 4 chlorines in positions 3,5 and 3´ and 5´, and two hydroxyethyl groups in positions 2 and 2´. Its low IC_{50} means that ZmCKX1 can accept the hydroxyalkyl group in the same position where the amide group interacts with the active site.

Inhibition of ZmCKX4a and ZmCKX8

The inhibition of two other maize CKXs by the studied compounds exhibited a very similar pattern. Compounds **69–73** were rather weak inhibitors of these enzymes, with compound **71** being the strongest ligand. The inhibitory strength of compound **71** was markedly increased when another substituent was introduced into the 5´ position (compounds **75–78**). As in the case of the ZmCKX1, compounds **75–78** were the most potent inhibitors of both enzymes of all compounds presented in this work (IC_{50} = 50 – 180 nM). Consistent with the results obtained with ZmCKX1, omitting one or both chlorines or replacement of one or both of the chlorines with a fluorine atom decreased the CKX inhibition to varying degrees (compounds **79–84**). Interestingly, when the chlorines were omitted from molecule **77**, the decrease in inhibitory activity was much more pronounced than in the same case of compound **78** (compare the difference in IC_{50} of compounds **77** and **79** with the difference in IC_{50} of compounds **78** and **80**).

Regarding compounds **85–88**, none of the *N*-substituents of the amid group significantly altered the inhibitory strength when compared to parent compound 76. Interestingly, a replacement of the amide group with a carboxyl group did not decrease the inhibitory activity of compounds **90–92** (except for compound **92** with ZmCKX4a). This contrasts with the results achieved with ZmCKX1, where this change decreased the inhibitory activity 200 - 500 times. The enzymes ZmCKX4a and ZmCKX8 thus display wider ligand specificity to derivatives with a carboxyl group than ZmCKX1. Only in the case when the carboxyl group was esterified by the methyl group (**93**), the activity was lost. Changing the position of the amide group from position 2´ to position 3´ (**94** vs **71**) slightly decreased the activity.

Inhibition of AtCKX2

Among compounds **69–73**, the lowest IC_{50} exhibited compound **73**, not compound **71** as in the case of maize CKXs. This may mean that the enzyme AtCKX2 interacts with the amide group more readily than maize CKXs at the location where both enzymes interact with the hydroxyalkyl group (Fig. 1A), or if the amide group binds in AtCKX2 to the same site as in ZmCKX1, that AtCKX2 better tolerates the presence of the TFM group in the internal cavity. The first option seems more likely if we consider that AtCKX2 prefers inhibitors with smaller substituents (such as hydrogen) in both positions 3 and 5 to larger ones (such as fluorine/chlorine/ bromine) in the internal cavity as previously discussed (Nisler *et al*., 2022).

When the TFM group was introduced to the same phenyl ring that carried the amide group (compound **78**), the IC_{50} was improved 10 times compared to compound **73**. Similar or slightly higher IC_{50}s were obtained with compounds **75**, **76**, and **77**, where the TFM group was replaced by chlorine/bromine atom, and methoxy group, respectively. Even a little higher activity than compound **78** exhibited compound **80** (IC_{50} = 6 nM), which has no halogen directly attached to the phenyl rings. This result confirmed that even DPU derivatives without halogen atoms on the phenyl ring, which interacts with the inner cavity of AtCKX2, can be strong inhibitors. A similar situation can be observed by comparing the IC_{50}s of compounds **77**, **79**, and **82**–**84**, all of which carry the methoxy group in the 5´ position, and different numbers and types of halogen atoms in positions 3 and 5. Their IC_{50}s are very similar, ranging from 0.074 – 0.15 µM.

As with ZmCKX1, the combination of the amide group in position 2´ with the 2-hydroxyalkyl group in position 2 does not improve the ability to inhibit AtCKX2. It is rather the opposite (compare the IC_{50} of **98** and **81**).

Binding of CKX inhibitors at the active site of ZmCKX4a and ZmCKX8

ZmCKX8, together with ZmCKX1, belongs to a subgroup comprising charged glutamate residue at the entrance to the active site (E372 in ZmCKX8), while ZmCKX4a belongs to the other subgroup with smaller uncharged residue such as Ser, Gly, Val or Ala (A373 in ZmCKX4a) at that position. This affects both cytokinin specificity and electron acceptor preference (Kopečný *et al*., 2016) and it has been shown that it can significantly alter inhibitor binding (Kopečný *et al*., 2016, Nisler *et al*., 2021).

Six crystal structures of ZmCKX4a and ZmCKX8, in complex with four CKX inhibitors, namely compound **71** (PDB 8CJ9 and 8CKQ), compound **77** (PDB 8CK6 and 8CLW), compound **78** (PDB CKT) and compound **99** (PDB 8CM2) were solved up to 1.8 Å resolution. A summary of the refinement results and model statistics is given in Table S1. All novel CKX inhibitors analyzed adopt overall a nearly planar conformation (Fig. 2 and S2). The 3,5-dichlorophenyl moiety is always stacked over the isoalloxazine ring of the FAD cofactor via the π electron interactions. Both chlorine atoms establish several hydrophobic interactions in ZmCKX4a (Fig. S2). The benzamide ring is oriented toward the entrance of the active site and is stacked between sidechains of P421 and V370 in ZmCKX4a (I418 and V369 in ZmCKX8).

As compared to the previously studied ligands e.g. 2-hydroxyethyl DPUs (Nisler *et al*., 2021), the novel 2-amido ureas are by ~ 1Å less deep and only one nitrogen atom of the urea is bound to the active-site base aspartate (D170 in ZmCKX4a or D167 in ZmCKX8). The loss of the second H-bond is compensated by the amide group of the benzamide ring that establishes several H-bonds directly or indirectly via a water network to surrounding residues including D170, E285, E325, and R369 in ZmCKX4a or equivalent D167, E281, E324, and R368 in ZmCKX8. In the case of ZmCKX8, the E372 at the entrance directly interacts, strengthening the amide group's binding (Fig. 2A, 2B). In the case of ZmCKX4a, this interaction is absent.

The methoxy group (compound **77**, Fig. 2B, 2D) or TFM group (compounds **78**, Fig. 2E, and **99**, Fig. 2F) on the benzamide ring is located in the hydrophobic pocket surrounded by the two conserved tryptophan rings in line with previous observations of TDZ- and DPU-derivatives (Nisler *et al*., 2016, Nisler *et al*., 2021). In ZmCKX4a, the methoxy group establishes two hydrophobic interactions with sidechains of W389 and V377, while the TFM group makes an additional third interaction with V370 (Fig. S2). Identical residues are found

in ZmCKX8, namely W388 and V376. These hydrophobic interactions critically contribute to the binding and inhibitory strength of tested compounds as deduced from the IC_{50} values of compounds **79** and **80** (Table 1).

Finally, the presence of the 2-hydroxyethyl group at the 3,5-dichlorophenyl ring (compound **99**) results in a slight adjustment allowing both urea nitrogens to bind to the aspartate in the active site. However, the 2-hydroxyethyl group interacts with the same amino acid (D170 in ZmCKX4a) as the amide group, which is most probably the reason why inhibitors with both groups (compounds **95**–**99**) do not have a higher affinity (inhibitory activity) for the CKX enzymes.

Toxicity evaluation in Caenorhabditis elegans

Because data on the safety of new compounds are key indicators in the development of biostimulants, and most of the studied compounds contain halogen atoms, we tested them for toxicity to *Caenorhabditis elegans*, a model nematode free-living in soil, and to human skin fibroblast (BJ) cells.

Of the compounds **69**–**73**, compound **73** containing the TFM group, has the greatest negative effect (Fig. 3A). When the TFM group was introduced to the phenyl ring which carries the 2-amido group, the negative effect further increased (**78**). Compound **78** completely inhibited the reproduction of *C. elegans* in both tested concentrations, 5 μM and 50 μM, and its IC_{50} reached 2.7 μM. Apparently, it is the effect of the combination of the 3TFM group with the 3,5-dichlorophenyl group because the other compounds (**71, 74–77** and **80**) which carry just one of these groups are less toxic or nontoxic. In particular, compound **77**, which combines a methoxy group with an amide group, is the least toxic of compounds **74**–**77**, indicating the negative effect of combining halogens with an amide group on one phenyl ring. The toxicity of compound **78** is in perfect agreement with the previous result (see the toxicity of compound **52** in Nisler *et al*., 2022).

N-substitution of the amide group also seems to enhance the toxic effect of the compounds (compare the effect of compounds **76** and **85**–**88**). Replacing the amide group with a carboxylic acid group or a methyl ester group also enhanced the negative effect of the compounds (compare the effect of compounds **75–77** with that of **90**–**93**). The highest toxicity against *C. elegans* was determined for compound **94** (IC_{50} = 1.9 μM) which carries the amide group in position 3´ instead of 2´ (**71** vs **94**).

Toxicity evaluation in BJ (skin fibroblast) cells

Most of the tested compounds were not harmful to BJ cells at a concentration of 50 μM (Fig. 3B). Notably, compound **78** inhibited the metabolic activity of 60% of the cells, and apparently, it was again caused by the combination of TFM group with 3,5-dichlorophenyl group (compare the effect of compounds **77** and **78**). Other toxic compounds were **86**, **87**, and **88**, carrying the *N*-substitution of the amide group, which appears to be responsible for this effect (compare the activity of compounds **86-88** with that of **76** and **85**). Interestingly, halogenated compounds **90** and **91** showed no adverse effect on BJ cells, but compound **92,** carrying the methoxy group instead of halogens, did. The methyl ester group showed a very similar negative effect in the case of compound **93**. Compound **94** also exhibited the toxic effect on BJ cells as well as in the case of *C. elegans*, indicating that the amide group in position 3´ on this type of compound is generally more toxic than the amide group in position 2´ (**71** vs **94**).

Activity in plant tissue culture

We showed previously that CKX-inhibitors **19**, **21** and **52** enhanced the shoot-inducing ability of iP on tobacco leaf discs (Nisler et al., 2021; 2022), and that endogenous concentration of iP-type cytokinins was approximately 40% higher in discs treated by compound **52**. Likewise, *de novo* shoot formation occurred on poplar leaf explants when iP was combined with compounds **19** or **21** (Nisler et al., 2021). To analyze the activity of novel CKX inhibitors in plants, compound **77** was tested for its ability to induce shoot formation in the presence or absence of iP in five different plant species. The effect of compound **77** was compared with the effect of compound **19** (Nisler *et al*., 2021), which exhibits slightly lower CKX inhibitory activity. In *Lobelia*, the compound **77** (together with iP) induced the formation of 16 shoots on average, whereas compound **19** (together with iP) only induced the formation of 8 shoots on average (Table 2). A similar result was obtained in *Drosera*, with the difference that both compounds **19** and **77** induced shoot formation even without exogenous cytokinin. In *Plectranthus* compound **77** showed slightly higher activity than compound **19** when the CKX inhibitors were applied alone. When the compounds were applied together with iP their effect was similar, yielding an average of 3 shoots per explant. In *Lavandula* and *Sempervivum*, the effect of both compounds was none or very weak. However, in *Lavandula*, compound **77** exhibited at least some positive effects in combination with iP compared to the completely ineffective application of iP alone (Table 2, Fig. 4).

Interaction of CKX inhibitors with Arabidopsis cytokinin receptors

Compounds **19**, **77**, **81** and **82** were tested for their interaction with Arabidopsis cytokinin receptors AHK3 and AHK4. None of the compounds displaced *trans*-zeatin from either receptor type more strongly than the negative control, adenine (Fig. S3), showing that the compounds are not able to bind to the cytokinin binding site of the receptors. Expectably, none of the compounds thus activated either receptor type at any tested concentration in a bacterial receptor activation assay (Fig. S3). These results demonstrate that none of the tested compounds interacts with the AHK3 or AHK4 receptor.

The effect of CKX inhibitors on activation of ARR5:GUS

Among compounds **19**, **77**, **81**, and **82**, compound **82** exhibited the highest activity, reaching 19% and 15% of BAP activity at 10 and 1 μM concentrations, respectively (Fig. 4C and Table S3). Compounds **19** and **81**, both at 1 μM concentration, also significantly activated ARR5 expression, reaching 9% and 8% of BAP activity, respectively. Compound **77** was the least active. If we exclude that the expression of ARR5 was mediated through the activation of the AHK2 receptor (which has a very similar ligand specificity to AHK4 (Stolz et al., 2011)), we can conclude that the higher expression of ARR5 in the presence of the tested compounds was a consequence of a higher endogenous cytokinin level. We showed previously that compound **19** (without activating AHK4) induced expression of ARR5, ARR9 and ARR16 (Nisler et al., 2021).

*The effect of CKX inhibitor **82** and* trans*-zeatin on activation of* TCSv2:GUS

In the untreated seedlings, GUS activity was detected mainly in the root, weakly in the epidermal cells of blades of cotyledon, and selectively in epidermal cells around the trichome base in the first true leaves (Fig. S4A). In the root, the staining was strongest in its upper part and gradually weakened downward to the elongation zone. In the root tip, there was weak staining in the cells of the columella, the quiescent centre, and the cortex (Fig. 5A). In the shoot of seedlings treated with compound **82**, the weak signal of the epidermal cells was completely abolished, and a signal was visible at the cotyledon tip, around the hydathodes (Fig. S4B). However, the roots of the treated plants were stained with similar intensity in the rhizodermis throughout the whole root (including the maturation zone) until the beginning of the elongation zone, which was approximately four times shorter than that of the control plant (Fig. 5B). Notably, there was a distinct staining at the early differentiation zone, where we

observed the ectopic formation of long root hairs, that were much more abundant and longer than in control plants (Fig. 5B). In the root tip, the signal of the columella cells and quiescent centre was similar to the untreated plants. On the contrary, treatment with *trans*-zeatin caused strong staining of the entire meristematic zone, but very weak in the maturation/early differentiation zone (Fig. 5C), although the mature root under the hypocotyl, and differentiation zone where lateral roots emerge, were strongly stained (Fig. S4C). Even so, the root phenotypes of plants treated with compound **82** and *trans*-zeatin were very similar. To conclude, compound **82** had a very similar effect on root phenotype as *trans*-zeatin, while the distribution and level of expression of cytokinin sensor *TCSv2* was between that found in the control and the *tZ*-treated plants. These results clearly demonstrate the different regulation of cytokinin signalling along the root by cytokinin and CKX inhibitor.

The effect of CKX inhibitors on the growth of Arabidopsis seedlings under optimal and low nutrition conditions

To analyze the effect of selected CKX inhibitors, Arabidopsis seeds were germinated in the presence of compounds **81**, **82**, and **77**, and then transferred to optimal (full MS) and low nutrition (low MS) conditions. Their effect was compared to compound **19** from our previous work (Nisler *et al*., 2021). Under both nutritional levels, the final area and the absolute growth rate were the most sensitive parameters (Fig. 6, S5). Under optimal nutrient conditions, compound **82** exhibited the best effect on the growth of plants, which was very similar to that of the reference compound **19** (Fig. 6, S5). Both compounds, at 1 μM concentration, increased the plants' final area and absolute growth rate by approximately 50% (Fig. 6, S5). Compound **82** also improved the early seed establishment, whereas compound **19** reduced it (Fig. S5). Compound **81** also promoted plant growth, but the effect was weaker than observed with compound **82**. Compound **77** showed the lowest growth-promoting activity. None of the compounds affected the plant's greenness (Fig. S5).

Under low nutrient conditions, compound **82** was the most effective biostimulant allowing plants to reach bigger sizes (higher final size, perimeter, and absolute growth rate) when applied at 1 and 10 μM concentrations (Fig. 6 and S5). Compounds **19** and **81** gave unclear results, not showing a significant positive effect. Compound **77** at 10 μM concentration showed a weak positive effect on the growth. Under low MS, the compounds did not modify the greenness of the Arabidopsis seedlings (Fig. S5). Generally, compound **82** was the most potent plant growth regulator in this experiment. The images of Arabidopsis seedlings treated

by compound **82** are shown in Fig. 6 and S6 and show that compound **82** increased not only the final size of the plants but also the homogeneity of the growth of the plant population.

*The effect of CKX inhibitors **77** and **82** on the growth of oilseed rape*

To gain insight into whether compounds **77** and **82** (Fig. 7C) affect agronomically important crops, a 22-day experiment was carried out with oilseed rape in a growth chamber. Oilseed rape treated with any of the tested compounds grew faster (Fig. 7) and reached significantly higher fresh weights of shoots and roots, 20 days after treatment. Shoot growth was more pronounced than root growth in both cases. The mean fresh weight of shoots of plants treated with compounds **82** and **77** was 51% and 62% higher than that of control plants, respectively (Fig 7A). The mean fresh weight of roots of plants treated with compounds **82** and **77** was 26% and 44% higher than that of control plants, respectively (Fig 7B). Figures 7D and 7E also show that the treated plants grew faster because they had 4 true leaves, unlike the control plants. This is important because successful seedling establishment is the first critical step for crop production, and often determines the success or failure of the future harvest.

Discussion

This is the third (after Nisler *et al*., 2021 and 2022) and final work where our group recently described the development of novel CKX inhibitors derived from DPU. In this work, we combined new discoveries with the know-how published before to gain CKX inhibitors with the highest possible efficiency and the simplest structure. Thus, some compounds (**75–78**) exhibited IC_{50} towards ZmCKX1 in the sub-nanomolar range, which is approximately 20 to 50 times lower than it was reached previously (e.g. compound **52** vs **77**). For example, compound **19** (3TFM-2HE) has IC_{50} (ZmCKX1) = 100 nM, while compound **77** has IC_{50} (ZmCKX1) = 0.9 nM. The inhibitory strength of key compounds from this work to AtCKX2 was also significantly improved (compare the IC_{50} of compounds **19** and **52** to that of **75**–**83**). Introducing the amide group to compound **52** resulted in compound **78**, and a seventy-fold improvement in IC_{50} (with AtCKX2). The inhibitory strength of the key compounds against ZmCKX4a remained similar to that of compound **52** or improved when compared to compound **19** (Table 1).

However, as mentioned in the introduction, the efficiency of new compounds is important, but it is only a prerequisite for success. The current legislative practices place high demands on the safety and harmlessness of new compounds for the environment and human health.

For this reason, we have prepared several derivatives (compounds **79**–**84**) of the two most promising compounds (**77** and **78**) with various degrees of halogen substitutions and tested them all together for toxicity against human skin cells and soil nematode *C. elegans*. The data (Fig. 3) show that compound **78** is unsuitable for practical use, while other compounds – **77**, **80**, **81**, **82**, **83** – seem safe. Very interesting is compound **80**, which carries only a 3TFM group and an amide group. Results obtained with this compound confirm that a TFM group is indeed an excellent group in terms of increasing the effectiveness of biologically active compounds (compare the IC_{50}s of compounds **79** and **80**) as has been mentioned before (Leroux *et al*., 2008; Liu *et al*., 2022). Liu further noted that trifluoromethoxy-containing compounds constitute only about 1.5% and 2.5% of the corresponding fluorine-containing pharmaceutical drugs and agrochemicals, respectively, and that the key reason for the low representation is a lack of convenient synthetic methods and, therefore, high cost of preparation of trifluoromethoxy derivatives. Unfortunately, this is also true in the case of compounds **78** and **80**, where the starting material (2-amino-4-(trifluoromethoxy)benzamide) is expensive and excludes large-scale production. The same applies to compound **83**, for which 1-chloro-3-fluoro-5-isocyanatobenzene is needed.

For these reasons, further biological experiments with Arabidopsis seedlings were performed with compounds **19**, **77**, **81**, and **82**. Notably, their growth-promoting activity correlates with their ability to activate ARR5:GUS expression, i.e., compound **82** showed the highest activity in both assays, while compound **77** showed the lowest (Fig. 4C, 6). Compound **82** had also a significant positive effect on Arabidopsis growth under low-nutrition conditions (Fig. 6B, S5, S6), which demonstrates its ability to enhance nutrient use efficiency. This result is not so surprising when we consider that compound **82** significantly induced root hair growth in Arabidopsis seedlings (Fig. 5B), and root hairs increase root surface area, enhance the uptake of nutrients and water, and promote overall plant growth (Gilroy and Jones, 2000). It was also shown that cytokinin signalling promotes root hair growth (Zhang et al., 2016; Takatsuka et al., 2023), while inhibiting cellular growth in the entire elongation zone (Liu et al., 2022). Thus, our results are completely consistent with these reports. Since compound **82** did not interact with Arabidopsis cytokinin receptors, we can conclude that its effect on root growth was due to the upregulation of cytokinin signalling.

Accordingly, compound **82** also improved the growth of oilseed rape (Fig. 7), which like Arabidopsis belongs to the *Brassicaceae* family. Interestingly, compound **77** had a similar and significant growth-promoting effect on shoot of oilseed rape as compound **82**. Moreover,

both compounds significantly increased also root growth, which is not consistent with other reports, generally showing that not inhibition of CKX, but overexpression of CKX genes (i.e. lowered levels of cytokinins) promote root growth, and oppositely (Gao et al., 2014; Pospíšilová et al., 2016; Ramireddy et al. 2018; reviewed in Chen et al., 2020). These results suggest that compounds **77** and **82** may affect also the off-target proteins other than the CKX enzymes. It also seems that their effect may be a species-specific. The compounds, which differ in the presence of one chlorine atom, may also have different solubility in the aqueous environment and/or the ability to penetrate plant cells and organelles. In any case, both compounds seem to deserve our attention regarding future potential in agricultural applications.

To conclude, using structure-activity relationship studies and analysis of the structures of crystal complexes of CKX inhibitors bound to CKX enzymes, we defined suitable positions to modify on both rings of DPU and suitable substituents for these positions, the combination of which led to the development of compounds with the highest possible inhibitory activity against ZmCKX1, AtCKX2 and ZmCKX4a and simple chemical structure. Efficiency data, toxicological studies, and a general market analysis further allowed us to preselect several compounds with the highest commercial potential. These compounds are **19**, **77**, and **82**, and possibly also compounds **85-88**, in which the methoxy group could substitute bromine to reduce the number of halogen atoms in the molecule. Future studies shall focus on greenhouse experiments, field trials, and further eco/toxicological studies. The great advantage of these compounds is that their structure is quite simple and their effective dose per hectare will be between 0.1 and 1 gram. We see the highest potential of the CKX inhibitors in their use as abiotic stress protectants, nutrient use enhancers, and yield quality and quantity improvers, all of which are key aspects in agriculture that need to be constantly improved.

Acknowledgements

We acknowledge SOLEIL for the provision of synchrotron radiation facilities (proposals ID 20170872 and 20191181) in using PROXIMA beamlines.

Funding

This work was supported by grant no. 21-07661S from the Czech Science Foundation and by the Jean d'Alembert fellowship within the France 2030 program ANR-11-IDEX-0003 of the Agence Nationale de la Recherche (DK).

Author contributions

JN designed, synthesized, and characterized the compounds with LH's help; PK and RK performed the CKX inhibition study under the supervision of LS and DK. DZ provided ZmCKX4a enzyme. DK, PB, and SM performed the X-ray crystallographic study; NM and SPOW performed the plant tissue culture assays; AK performed the experiments with *C. elegans*; JV performed the experiments with human cells; MK performed the TSCv2:GUS experiment. NDD and LS performed the assay with Arabidopsis seedlings. MCh performed the experiment with oilseed rape. JN designed the research and wrote the paper with contributions by co-authors. All the authors provided editorial changes to the manuscript and approved its submission.

Conflict of interest

Authors of this manuscript (JN, DK, and LS) are authors of these patents CZ2020143A3; EP4120837A1; and WO2021185390A1, which claim the protection of several compounds described in this paper and their use as plant growth regulators.

Data availability

Data reporting crystal structures are publicly accessible in the Protein Data Bank archive. Two ZmCKX8 inhibitor complexes with compounds **71** and **77** are under accession codes 8CJ9 and 8CK6, respectively. Four ZmCKX4a inhibitor complexes with compounds **71**, **77**, **78**, and **99** are deposited under accession codes 8CKQ, 8CLW, 8CKT, and 8CM2, respectively.

References

Aremu AO, Masondo NA, Sunmonu TO, Kulkarni MG, Zatloukal M, Spichal L, Doležal K, Van Staden J. 2014. A novel inhibitor of cytokinin degradation (INCYDE) influences the biochemical parameters and photosynthetic apparatus in NaCl-stressed tomato plants. Planta 240, 877–889.

Ashikari M, Sakakibara H, Lin S, Yamamoto T, Takashi T, Nishimura A, Angeles ER, Qian Q, Kitano H, Matsuoka M. 2005. Cytokinin oxidase regulates rice grain production. Science 309, 741–745.

Bartrina I, Otto E, Strnad M, Werner T, Schmülling T. 2011. Cytokinin regulates the activity of reproductive meristems, flower organ size, ovule formation, and thus seed yield in *Arabidopsis thaliana*. Plant Cell 23, 69–80.

Camblin P, Kon KF, Leipner J, Schmitt N, Thayumanavan AB. 2017. Abiotic stress tolerance. WO 2017/216003.

Camblin P, Pingel A. 2017. Pesticidal compositions. WO 2017/215981.

Chatfeld JM, Armstrong DJ. 1986. Regulation of cytokinin oxidase activity in callus tissues of Phaseolus vulgaris L. cv Great Northern. Plant Physiology 80, 493–499.

Chen L, Zhao J, Song J, Jameson PE. 2020. Cytokinin dehydrogenase: a genetic target for yield improvement in wheat. Plant Biotechnology Journal 3, 614-630.

De Diego N, Fürst T, Humplík JF, Ugena L, Podlešáková K, Spíchal L. 2017. An Automated Method for High-Throughput Screening of Arabidopsis Rosette Growth in Multi-Well Plates and Its Validation in Stress Conditions. Frontiers in Plant Science 8, 01702.

De Resende PE, Nisler J, Voller J, Kadlecová A, Gibbons S. 2023. Antimicrobial and anthelmintic activities of aryl urea agents. Journal of Global Antimicrobial Resistance 33, 114-119.

Frébortová J, Galuszka P, Werner T, Schmülling T, Frébort I. 2007. Functional expression and purification of cytokinin dehydrogenase from Arabidopsis thaliana (AtCKX2) in *Saccharomyces cerevisiae*. Biologia Plantarum 51, 673–682.

Galuszka P, Popelková H, Werner T, Frébortová J, Pospíšilová H, Mik V, Köllmer I, Schmülling T, Frébort I. 2007. Biochemical characterization and histochemical localization

of cytokinin oxidases/dehydrogenases from *Arabidopsis thaliana* expressed in *Nicotiana tabaccum* L. Journal of Plant Growth Regulation 26, 255–267.

Gao S, Fang J, Xu F *et al.* 2014. CYTOKININ OXIDASE/DEHYDROGENASE4 integrates cytokinin and auxin signaling to control rice crown root formation. Plant Physiology 165, 1035–1046.

Gemrotová M, Kulkarni MG, Stirk WA, Strnad M, Van Staden J, Spíchal L. 2013. Seedlings of medicinal plants treated with either a cytokinin antagonist (PI-55) or an inhibitor of cytokinin degradation (INCYDE) are protected against the negative effects of cadmium. Plant Growth Regulation 71, 137–145.

Gilroy S, Jones DL. 2000. Through form to function: root hair development and nutrient uptake. Trends in Plant Science 5, 56–60.

Hare PD, Van Staden J. 1994. Inhibitory effect of thidiazuron on the activity of cytokinin oxidase isolated from soybean callus. Plant Cell Physiology 35, 1121–1125.

Houba-Hérin N, Pethe C, d'Alayer J, Laloue M. 1999. Cytokinin oxidase from *Zea mays*: purification, cDNA cloning and expression in moss protoplasts. Plant Journal 17, 615-626.

Jefferson RA, Kavanagh TA and Bevan MW. 1987. GUS fusions: Beta-glucuronidase as a sensitive and versatile gene fusion marker in higher plants. The EMBO Journal 6: 3901–3907.

Khan MIR, Jalil SU, Chopra P, Chhillar H, Ferrante A, Khan NA, Ansari MI. 2021. Role of GABA in plant growth, development and senescence. Plant Gene 26, 100283.

Kieber JJ, Schaller GE. 2014. Cytokinins. The Arabidopsis Book 12, e0168.

Kon KF, Leipner J, Schmitt N, Thayumanavan AB. 2017. Use of 6-anilino purine derivatives to improve heat stress tolerance of rice seedlings. WO 2017/216005.

Kopečný D, Končitíková R, Popelka H, *et al.* 2016. Kinetic and structural investigation of the cytokinin oxidase/dehydrogenase active site. FEBS J. 283, 361-77.

Leroux FR, Manteau B, Vors JP, Pazenok S. 2008. Trifluoromethyl ethers-synthesis and properties of an unusual substituent. Beilstein Journal of Organic Chemistry 4, 13.

Li MF, Guo SJ, Yang XH, Meng QW, Wei XJ. 2016. Exogenous gamma-aminobutyric acid increases salt tolerance of wheat by improving photosynthesis and enhancing activities of antioxidant enzymes. Biologia Plantarum 60, 123-131.

Liu J, Lin W, Sorochinsky AE, Butler G, Landa A, Han J, Soloshonok VA. 2022. Successful trifluoromethoxy-containing pharmaceuticals and agrochemicals. Journal of Fluorine Chemistry 257–258, 109978.

Liu S, Strauss S, Adibi M, Mosca G, Yoshida S, Ioio RD, Runions A, Andersen TG, Grossmann G, Huijser P. 2022. Cytokinin promotes growth cessation in the Arabidopsis root. Current Biology 32, 1974-1985.

Merewitz EB, Du H, Yu W, Liu Y, Gianfagna T and Huang B. 2012. Elevated cytokinin content in ipt transgenic creeping bentgrass promotes drought tolerance through regulating metabolite accumulation. Journal of Experimental Biology 15, 1315–1328.

Morris RO, Bilyeu KD, Laskey JG, Cheikh NN. 1999. Isolation of a gene encoding a glycosylated cytokinin oxidase from maize. Biochemical and Biophysical Research Communications 255, 328–333.

Nisler J, Kopečný D, Končitíková R, Zatloukal M, Bazgier V, Berka K, Zalabák D, Briozzo P, Strnad M, Spíchal L. 2016. Novel thidiazuron-derived inhibitors of cytokinin oxidase/dehydrogenase. Plant Molecular Biology 92, 235–248.

Nisler J, Kopečný D, Pěkná Z, *et al.* 2021. Diphenylurea-derived cytokinin oxidase/ dehydrogenase inhibitors for biotechnology and agriculture. Journal of Experimental Botany 72, 355–370.

Nisler J, Pěkná Z, Končitíková R, *et al.* 2022. Cytokinin oxidase/dehydrogenase inhibitors: outlook for selectivity and high efficiency, Journal of Experimental Botany 73, 4806–4817.

Nisler J, Zatloukal M, Popa I, Dolezal K, Strnad M, Spíchal L. 2010. Cytokinin receptor antagonists derived from 6-benzylaminopurine. Phytochemistry 71, 823–30.

Podlešáková K, Ugena L, Spíchal L, Doležal K, De Diego N. 2019. Phytohormones and polyamines regulate plant stress responses by altering GABA pathway. New Biotechnology 48, 53–65.

Pospíšilová H, Jiskrová E, Vojta P, *et al.* 2016. Transgenic barley overexpressing a cytokinin dehydrogenase gene shows greater tolerance to drought stress. New Biotechnology 33, 692–705.

Ramireddy E, Hosseini SA, Eggert K, Gillandt S, Gnad H, von Wiren N, Schmuelling T. 2018. Root engineering in barley: increasing cytokinin degradation produces a larger root system, mineral enrichment in the shoot and improved drought tolerance. Plant Physiology 177, 1078–1095.

Romanov GA, Kieber JJ, Schmülling T. 2002. A rapid cytokinin response assay in Arabidopsis indicates a role for phospholipase D in cytokinin signalling. FEBS Letters. 515, 39–43.

Romanov GA, Spíchal L, Lomin SN, Strnad M, Schmülling T. 2005. A live cell hormone-binding assay on transgenic bacteria expressing a eukaryotic receptor protein. Analytical Biochemistry 347, 129–134.

Seifikalhor M, Aliniaeifard S, Bernard F, Seif M, Latifi M, Hassani B, Didaran F, Bosacchi M, Rezadoost H, Li T. 2020. γ-Aminobutyric acid confers cadmium tolerance in maize plants by concerted regulation of polyamine metabolism and antioxidant defense systems. Scientific Reports 10, 3356.

Spíchal L, Rakova NY, Riefler M, Mizuno T, Romanov GA, Strnad M et al. 2004. Two cytokinin receptors of Arabidopsis thaliana, CRE1/ AHK4 and AHK3, differ in their ligand specificity in a bacterial assay. Plant Cell Physiology 45, 1299–1305.

Steiner E, Israeli A, Gupta R, et al. 2020. Characterization of the cytokinin sensor TCSv2 in arabidopsis and tomato. Plant Methods 16, 152.

Stolz A, Riefler M, Lomin SN, Achazi K, Romanov GA, Schmülling T. 2011. The specificity of cytokinin signalling in Arabidopsis thaliana is mediated by differing ligand affinities and expression profiles of the receptors. Plant J. 67, 157-68.

Suzuki T, Miwa K, Ishikawa K, Yamada H, Aiba H, Mizuno T. 2001. The Arabidopsis sensor His-kinase, AHK4, can respond to cytokinins. Plant Cell Physiology 42, 107–113.

Šmehilová M, Galuszka P, Bilyeu KD, Jaworek P, Kowalska M, Šebela M, Sedlářová M, English JT, Frébort I. 2009. Subcellular localization and biochemical comparison of cytosolic and secreted cytokinin dehydrogenase enzymes from maize. Journal of Experimental Botany 60, 2701–2712.

Takatsuka H, Sasaki A, Takahashi N, Shibata M, Sugimoto K, Tanaka M, Seki M, Umeda M. 2023. Cytokinin signaling promotes root hair growth by directly regulating RSL4 expression. Journal of Experimental Botany 74, 3579–3594.

Ugena L, Hýlová A, Podlešáková K, Humplík JF, Doležal K, Diego N, Spíchal L. 2018. Characterization of biostimulant mode of action using novel multi-trait high-throughput screening of Arabidopsis germination and rosette growth. Frontiers in Plant Science 9, 1327.

Voller J, Zahajská L, Plíhalová L, *et al*. 2019. 6-Substituted purines as ROCK inhibitors with anti-metastatic activity, Bioorganic Chemistry 90, 103005.

Vyroubalová Š, Václavíková K, Turečková V, Novák O, Šmehilová M, Hluska T, Ohnoutková L, Frébort I, Galuszka P. 2009. Characterization of new maize genes putatively involved in cytokinin metabolism and their expression during osmotic stress in relation to cytokinin levels. Plant Physiology 151, 433–447.

Wang Y, Gu W, Meng Y, Xie T, Li L, Li J, Wei S. 2017. γ-Aminobutyric acid imparts partial protection from salt stress injury to maize seedlings by improving photosynthesis and upregulating osmoprotectants and antioxidants. Scientific Reports 7, 43609.

Werner T, Motyka V, Laucou V, Smets R, Van Onckelen H, Schmülling T. 2003. Cytokinin-deficient transgenic Arabidopsis plants show multiple developmental alterations indicating opposite functions of cytokinins in the regulation of shoot and root meristem activity. Plant Cell 15, 2532–2550.

Yamada H, Suzuki T, Terada K, Takei K, Ishikawa K, Miwa K, et al. 2001. The Arabidopsis AHK4 histidine kinase is a cytokinin-binding receptor that transduces cytokinin signals across the membrane. Plant Cell Physiology 42, 1017–1023.

Zalewski W, Galuszka P, Gasparis S, Orczyk W, Nadolska-Orczyk A. 2010. Silencing of the *HvCKX1* gene decreases the cytokinin oxidase/dehydrogenase level in barley and leads to higher plant productivity. Journal of Experimental Botany 61, 1839–51.

Zhang S, Huang L, Yan A, Liu Y, Liu B, Yu C, Zhang A, Schiefelbein J, Gan Y. 2016. Multiple phytohormones promote root hair elongation by regulating a similar set of genes in the root epidermis in Arabidopsis. Journal of Experimental Botany 67, 6363–6372.

Tables

Table 1. Structures of diphenylurea derivatives prepared, and an overview of their IC_{50} values measured with four CKX isoforms.

Diphenylurea derivatives					IC_{50} (μM)			
Compound	R substituents				ZmCKX1	ZmCKX4a	ZmCKX8	AtCKX2
of structure B	R3	R5	R5´	R				
19	**3TFM – 2HE**				0.10 ± 0.01	1.5 ± 0.07	0.19 ± 0.01	0.23 ± 0.01
52	**Cl**	**Cl**	**OCF_3**		0.017 ± 0.003	0.030 ± 0.004	-	0.75 ± 0.07
69	**Cl**	H	H	**NH_2**	0.32 ± 0.06	71 ± 2	21 ± 0	1.3 ± 0.1
70	**Cl**	**F**	H	**NH_2**	0.065 ± 0.008	9.5 ± 1.0	5.0 ± 0.4	0.76 ± 0.11
71 (2AD-3,5DCl)	**Cl**	**Cl**	H	**NH_2**	0.015 ± 0.004	2.5 ± 0.5	1.2 ± 0.1	0.34 ± 0.02
72	**Cl**	**CH_3**	H	**NH_2**	0.050 ± 0.007	9.0 ± 2.3	5.4 ± 1.8	0.81 ± 0.14
73	**Cl**	**OCF_3**	H	**NH_2**	0.083 ± 0.011	> 100	N.A.	0.11 ± 0.03
74	**4 x Cl in 3,5, 3´,5´**			**NH_2**	0.055 ± 0.23	-	-	> 100
75	**Cl**	**Cl**	**Cl**	**NH_2**	0.00091 ± 0.0001	0.051 ± 0.004	0.075 ± 0.014	0.019 ± 0.002
76	**Cl**	**Cl**	**Br**	**NH_2**	0.00065 ± 0.0001	0.13 ± 0.01	0.21 ± 0.10	0.019 ± 0.001
77 (2AD,5OMe-3,5DCl)	**Cl**	**Cl**	**OCH_3**	**NH_2**	0.00087 ± 0.0001	0.065 ± 0.011	0.18 ± 0.01	0.074 ± 0.010
78	**Cl**	**Cl**	**OCF_3**	**NH_2**	0.00075 ± 0.0001	0.053 ± 0.017	0.13 ± 0.01	0.011 ± 0.003
79	H	H	**OCH_3**	**NH_2**	0.12 ± 0.01	80 ± 20	18 ± 1	0.088 ± 0.022
80	H	H	**OCF_3**	**NH_2**	0.011 ± 0.002	1.0 ± 0.1	0.7 ± 0.03	0.006 ± 0.003
81 (2AD,5Cl-3Cl)	**Cl**	H	**Cl**	**NH_2**	0.18 ± 0.07	6.0 ± 1.5	-	0.76 ± 0.14

82 (2AD,5OMe-3Cl)	**Cl**	H	**OCH_3**	**NH_2**	0.023 ± 0.015	2.5 ± 0.3	0.88 ± 0.01	0.088 ± 0.015
83	**Cl**	**F**	**OCH_3**	**NH_2**	0.005 ± 0.0004	0.11 ± 0.02	0.34 ± 0.06	0.084 ± 0.004
84	**F**	**F**	**OCH_3**	**NH_2**	0.019 ± 0.0011	0.63 ± 0.20	0.51 ± 0.04	0.15 ± 0.03
85	**Cl**	**Cl**	**Br**	**NH-Et**	0.0021 ± 0.0005	0.17 ± 0.01	0.15 ± 0.02	0.25 ± 0.02
86	**Cl**	**Cl**	**Br**	**NH-EtOH**	0.0025 ± 0.0003	0.12 ± 0.01	0.20 ± 0.02	0.33 ± 0.01
87	**Cl**	**Cl**	**Br**	**NH-$EtNH_2$**	0.009 ± 0.001	0.18 ± 0.08	0.35 ± 0.01	0.94 ± 0.10
88	**Cl**	**Cl**	**Br**	**NH-NH_2**	0.014 ± 0.008	0.19 ± 0.02	0.30 ± 0.05	0.46 ± 0.08
89	**Cl**	**Cl**	H	**NH-OH**	0.65 ± 0.05	-	N.A.	6.3 ± 0.6
90	**Cl**	**Cl**	**Cl**	**OH**	0.27 ± 0.10	0.12 ± 0.2	0.19 ± 0.01	1.8 ± 0.4
91	**Cl**	**Cl**	**Br**	**OH**	0.14 ± 0.03	0.39 ± 0.06	0.21 ± 0.03	1.8 ± 0.3
92	**Cl**	**Cl**	**OCH_3**	**OH**	0.49 ± 0.14	0.87 ± 0.05	0.33 ± 0.06	7.3 ± 1.6
93	**Cl**	**Cl**	**OCH_3**	**OCH_3**	0.63 ± 0.22	45 ± 13	> 100	> 100
94 (3AD-3,5DCl)	**Cl**	**Cl**	H	**3-$CONH_2$**	0.22 ± 0.04	9.3 ± 1.7	3.2 ± 1.0	3.4 ± 0.5
Structure C	R3	R5	R5´	n				
95	H	H	H	2	5.5 ± 0.7	-	-	11 ± 2
96	H	H	**Cl**	2	0.070 ± 0.01	-	-	0.10 ± 0.02
97	H	**Cl**	**Cl**	1	0.045 ± 0.02	-	-	0.34 ± 0.05
98	H	**Cl**	**OCH_3**	2	0.052 ± 0.01	-	-	1.5 ± 0.1
99	**Cl**	**Cl**	**OCF_3**	2	0.004	1.0 ± 0.3	-	0.15
100	(structure in supplement)				0.12 ± 0.03	3.4 ± 1.0	-	2.8 ± 0.3
101	(structure in supplement)				0.015 ± 0.006	0.35 ± 0.04	0.80	0.38 ± 0.04

102	(structure in supplement)	54 ± 12	-	-	> 100
103	(structure in supplement)	11 ± 5	-	-	> 100

AtCKX2 and ZmCKX1 inhibition assays were performed using 2,6-dichlorophenolindophenol as an electron acceptor. ZmCKX8 and ZmCKX4a inhibition assays were performed using PMS/MTT reaction mixture. The values presented for compounds **19** and **52** have been published previously (Nisler et al., 2021; 2022) and are shown for comparison. Errors show the SD of at least two independent assays, each consisting of at least two replicates. Structures B and C correspond with Fig. 1B and 1C, respectively. N.A. – not active, - – not tested.

Table 2. Mean number of shoots per treatment.

Species	Control	1 µM iP	1 µM 19	1 µM iP + 1 µM 19	1 µM 77	1 µM iP + 1 µM 77
Lobelia	0	1.3 ± 0.7 a	0	8.4 ±3.4 b	0.6 ±0.4 ab	16.4 ±4.1 c
Drosera	0.7 ± 0.3 a	1.5 ± 0.6 a	6.2 ± 0.9 b	8.8 ± 2.0 b	7.0 ± 1.7 b	12.5 ± 1.8 c
Plectranthus	0	1.0 ±0.1 a	0.1 ±0.1 a	3.4 ±0.6 b	1.5 ±0.4 a	3.1 ±1.4 b
Lavandula	0	0	0	0	0.1 ± 0.1 a	0.3 ± 0.2 a
Sempervivum	0.3 ± 0.15 ab	0.2 ± 0.1 ab	0.6 ± 0.16 b	0.4 ± 0.16 ab	0.1 ± 0.1 a	0

Values represent mean (n = 20, ± SE). Means with different letters per row represent statistically significant differences in the Duncan's test at $P \leq 0.05$. The entire experiment was performed once in two independent replicates, each with ten explants for each treatment per plant species.

Figure legends

Fig. 1. Structures of the cytokinin oxidase/dehydrogenase inhibitors tested in the study. (A) Top view of the compound **19** bound to ZmCKX4a visualized using PyMOL software (PDB ID: 6YAO; Nisler *et al*., 2021). The red arrow indicates the entrance to the active site. (B) Structure of compounds **69–93**. The numbering of the positions of phenyl carbon atoms used in this work is shown. (C) Structure of compounds **94–98**. (D) Structures of key compounds **19** and **52** from Nisler et al. 2021; 2022 and from this work (**71–86**). The IC_{50} values presented were determined with ZmCKX1.

Fig. 2. Binding of diphenyl urea derivatives in the active site of ZmCKX. (A) Compound **71** (in blue) bound in the active site of ZmCKX8 (in cyan), (B) compound **77** (in green) bound in the active site of ZmCKX8, (C) Compound **71** (in blue) bound in the active site of ZmCKX4a (in grey), (D) compound **77** (in green) bound in the active site of ZmCKX4a, (E) Compound **78** (in light brown) bound in the active site of ZmCKX4a, (F) Compound **99** (in magenta) bound in the active site of ZmCKX4a. All inhibitors are shown in a Fo – Fc omit map contoured at 3.0 σ. The FAD cofactor is colored yellow and neighboring residues are labeled. Hydrogen bonds are shown as dashed lines.

Fig. 3. Evaluation of toxicity of compounds on *Caenorhabditis elegans* (A) and skin fibroblasts (BJ) cells (B). Nematode cultures were treated with the compounds at either 5 μM or 50 μM for 4 d and toxicity was determined by chitinase assay, which provides a measure of the ability of worms to produce healthy eggs. BJ cell cultures were treated with the compounds at 50 μM for 3 d and viability was determined using a resazurin reduction assay, measuring the metabolic activity of the cell population. In (A) and (B), the percentage values are the means of three independent experiments (± SD), and the means are relative to the control sample containing 0.2% DMSO. In (A) and (B) ivermectin (0.5 μM) and N^6-benzyladenosine (5 μM) were used as positive controls, respectively, reducing the reproductive capacity/viability to less than 10%. Statistically significant differences between the control sample (DMSO) and treatments, determined using the two- tailed Student's t- test are indicated with *a*, *b* or *c*, corresponding to *P*-values of $0.05 > P > 0.01$, $0.01 > P > 0.001$, and $P < 0.001$, respectively. Red arrows help to identify the same compounds with high toxic effects in both assays. Compound abbreviations have been used for better orientation in the results. The numbers show the positions of the substituents on the phenyl rings. Substituent abbreviations are derived from their element symbol in Mendeleev's table (halogens) or their

chemical names (groups); AD – amide, D – di, Me – methyl, TFM – trifluoromethoxy, OMe – methoxy, ED – ethyl amide, HED – hydroxyethyl amide, AED – aminoethyl amide, HD – hydrazide, HA – hydroxamic acid, CA – carboxylic acid, ME – methyl ester.

Fig. 4. Biological activity of tested compounds in different plant species. Effect of combinations of N^6-isopentenyladenine (iP) and compounds **19** and **77** on adventitious shoot regeneration of *Lobelia* (A) and *Lavandula* (B). The experiments were performed once with 20 explants for each treatment and the presented pictures are representative examples. (C) Effect of selected compounds on activation of *ARR5:GUS* in transgenic Arabidopsis plants (*ARR5* is a cytokinin primary response gene). BAP (N^6-benzylaminopurine) was used as a standard (positive control) and 0.1% DMSO as a blank control (set as 0%, dashed line). The means are relative to the activity of BAP, which was set as 100%. Error bars show the SD of the mean of two independent experiments, each performed in triplicate. Asterisks indicate statistically significant differences identified by the two- tailed Student's t- test at $P < 0.05$. The exact values are in Table S2.

Figure 5. The effect of compound **82** and *trans*-zeatin on GUS activity in the part of the root of 8-days-old Arabidopsis seedlings with *TCSv2:uidaA (TWO-COMPONENT OUTPUT SENSOR VERSION2)* reporter gene. Plants were cultivated in the presence of 0.01% DMSO (control) (A), 1 μM compound **82** (B) or 1 μM trans-zeatin (C) in a growth medium. The upper pictures show the root with root hairs above the root tip, and the bottom pictures show the root tip divided into the maturation, elongation, and meristematic zones, respectively. Pictures of the whole seedlings are in Fig. S4.

Figure 6. The effect of selected compounds on the final green leaf area of 11-day-old Arabidopsis seedlings on full (A) and low (B) MS. Compounds were tested in 0.01, 0.1, 1 and 10 μM concentrations as indicated. DMSO (0.1%) was used as solvent control (dashed line). The error bars show the SE of the mean (n = 48) from one experiment. Statistically significant differences between control (DMSO) and treatments identified by the two- tailed Student's t-test are indicated by the letters *a*, *b*, or *c*, corresponding to *P*-values of $0.05 > P > 0.01$, $0.01 > P > 0.001$, and $P < 0.001$, respectively. The inserts show that compound **82** increases shoot growth and the homogeneity of the seedling population. Pictures of the whole plates are in Fig. S5. Detailed analysis of the other plant characteristics is in Fig. S5. MS – Murashige and Skoog medium.

Fig. 7. Effect of compounds **77** and **82** on the growth of winter oilseed rape. (A) Shoot fresh weight. (B) Root fresh weight. (C) Structures of compounds **77** and **82**. (D, E) Photograph of average control plant (D) and average plant treated with 100 nM compound **82** (E). The plants were 22 days old. In (A, B) Statistically significant differences between means of control and treatments (n = 12 ± SD) identified by the two- tailed Student's t- test are indicated by the letters *a*, *b*, or *c*, corresponding to *P*-values of $0.05 > P > 0.01$, $0.01 > P > 0.001$, and $P < 0.001$, respectively. The entire experiment was performed one time.

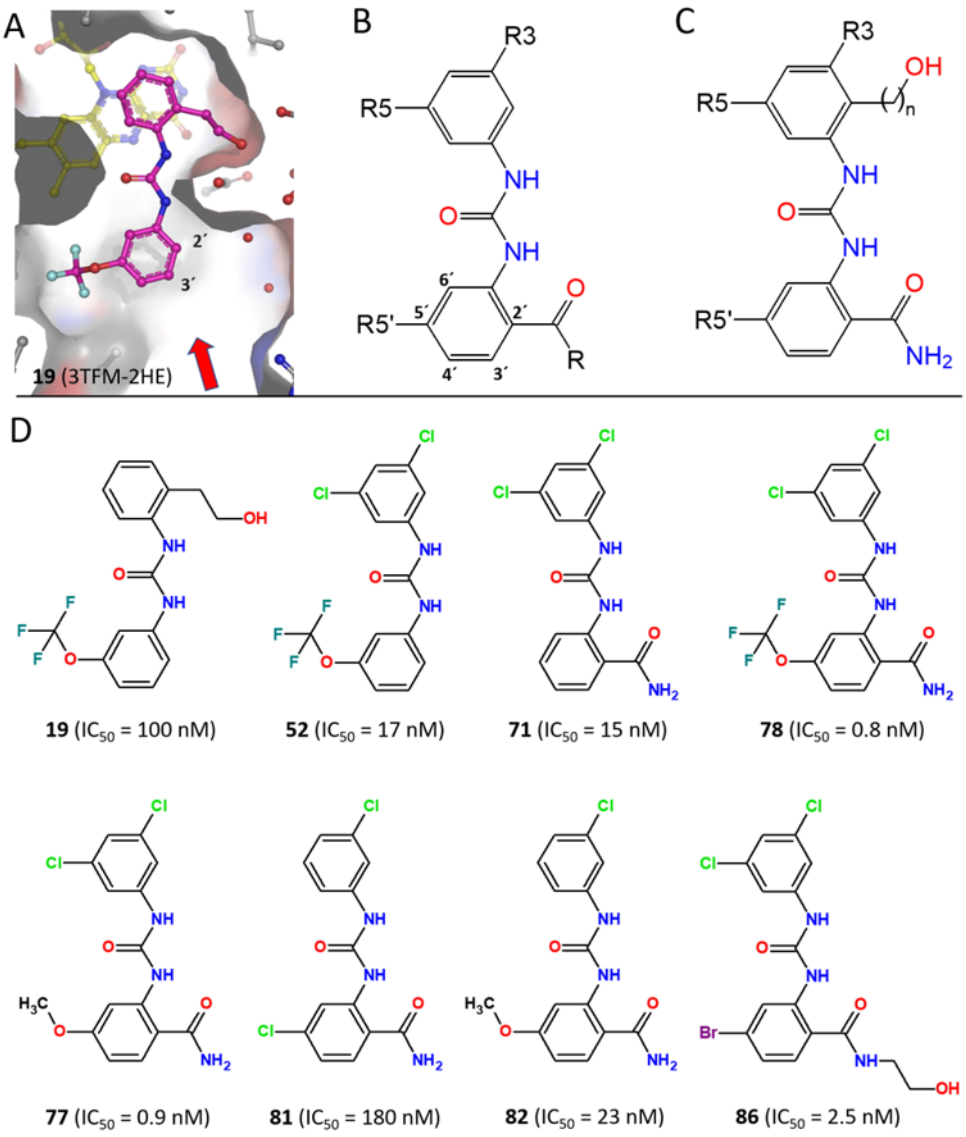

Fig. 1. Structures of the cytokinin oxidase/dehydrogenase inhibitors tested in the study. (A) Top view of the compound **19** bound to ZmCKX4a visualized using PyMOL software (PDB ID: 6YAO; Nisler *et al*., 2021). The red arrow indicates the entrance to the active site. (B) Structure of compounds **69–93**. The numbering of the positions of phenyl carbon atoms used in this work is shown. (C) Structure of compounds **94–98**. (D) Structures of key compounds **19** and **52** from Nisler et al. 2021; 2022 and from this work (**71–86**). The IC_{50} values presented were determined with ZmCKX1.

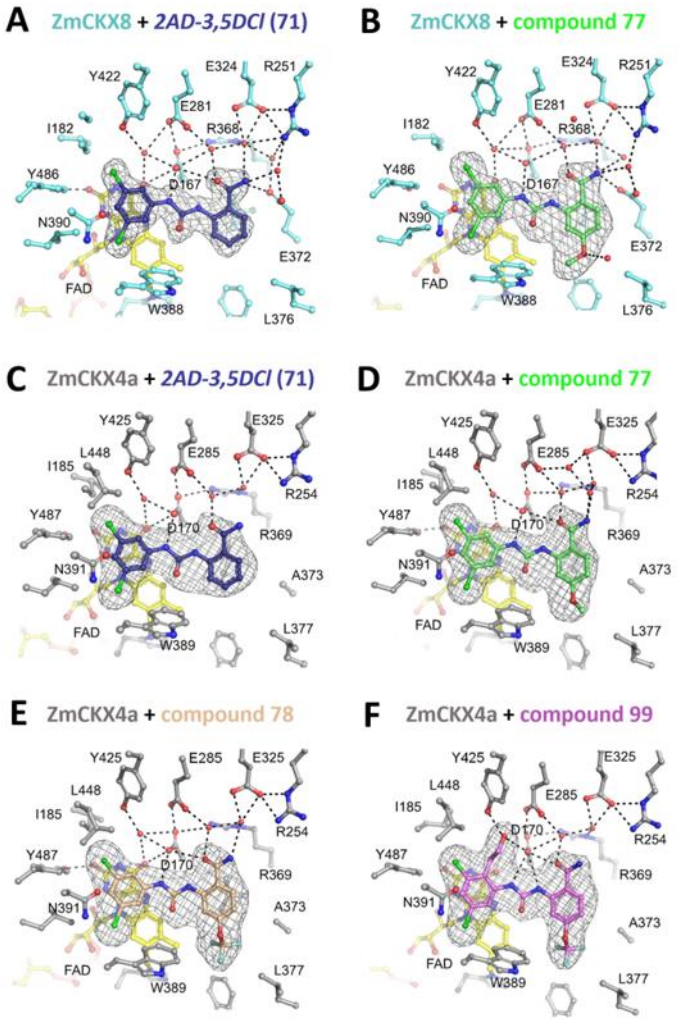

Fig. 2. Binding of diphenyl urea derivatives in the active site of ZmCKX. (A) Compound **71** (in blue) bound in the active site of ZmCKX8 (in cyan), (B) compound **77** (in green) bound in the active site of ZmCKX8, (C) Compound **71** (in blue) bound in the active site of ZmCKX4a (in grey), (D) compound **77** (in green) bound in the active site of ZmCKX4a, (E) Compound **78** (in light brown) bound in the active site of ZmCKX4a, (F) Compound **99** (in magenta) bound in the active site of ZmCKX4a. All inhibitors are shown in a Fo – Fc omit map contoured at 3.0 σ. The FAD cofactor is colored yellow and neighboring residues are labeled. Hydrogen bonds are shown as dashed lines.

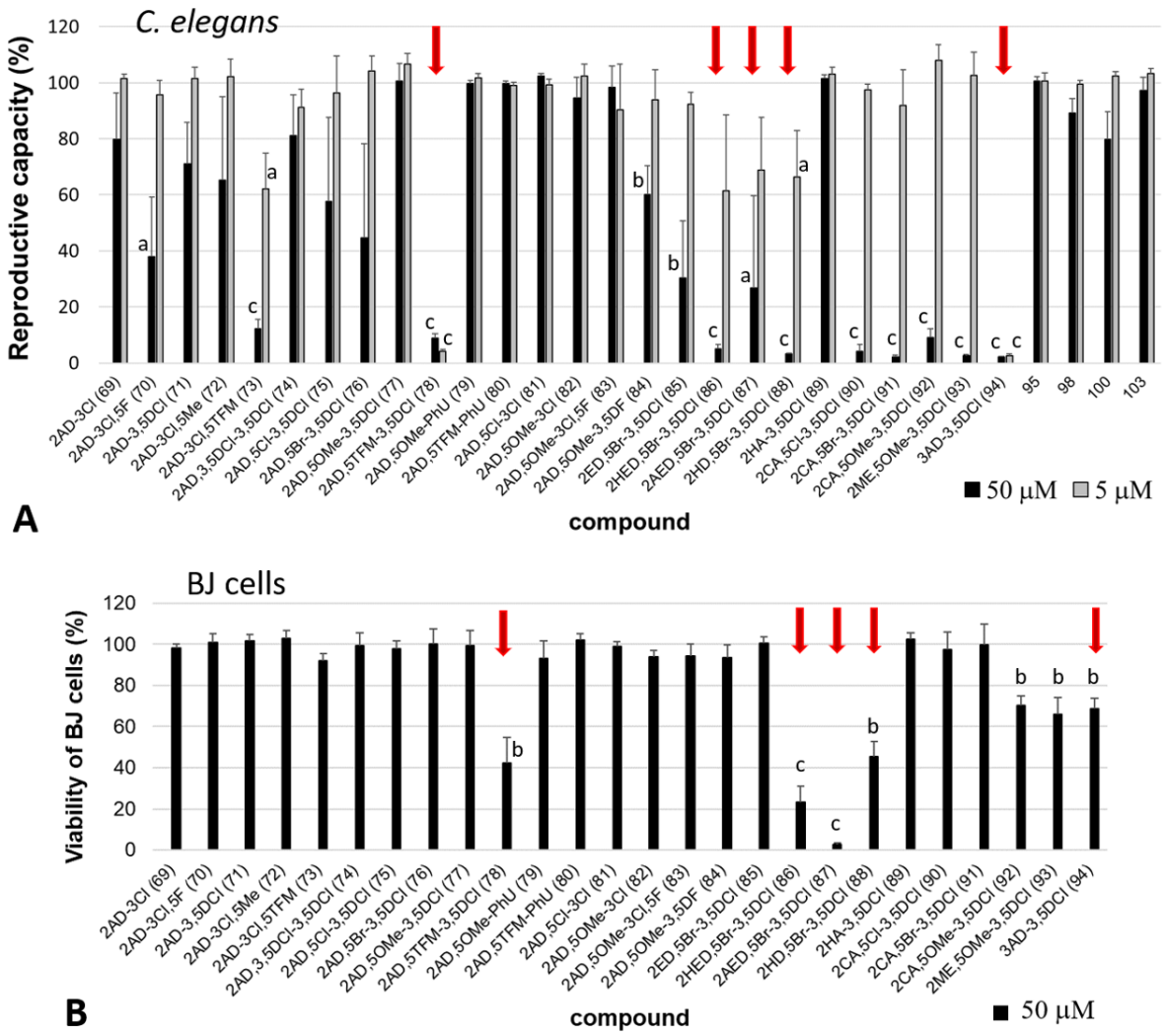

Fig. 3. Evaluation of toxicity of compounds on Caenorhabditis elegans (A) and skin fibroblasts (BJ) cells (B). Nematode cultures were treated with the compounds at either 5 µM or 50 µM for 4 d and toxicity was determined by chitinase assay, which provides a measure of the ability of worms to produce healthy eggs. BJ cell cultures were treated with the compounds at 50 µM for 3 d and viability was determined using a resazurin reduction assay, measuring the metabolic activity of the cell population. In (A) and (B), the percentage values are the means of three independent experiments (± SD), and the means are relative to the control sample containing 0.2% DMSO. In (A) and (B) ivermectin (0.5 ?M) and N6-benzyladenosine (5 ?M) were used as positive controls, respectively, reducing the reproductive capacity/viability to less than 10%. Statistically significant differences between the control sample (DMSO) and treatments, determined using the two-tailed Student's t-test are indicated with a, b or c, corresponding to P-values of $0.05 > P > 0.01$, $0.01 > P > 0.001$, and $P < 0.001$, respectively. Red arrows help to identify the same compounds with high toxic effects in both assays. Compound abbreviations have been used for better orientation in the results. The numbers show the positions of the substituents on the phenyl rings. Substituent abbreviations are derived from their element symbol in Mendeleev's table (halogens) or their chemical names (groups); AD – amide, D – di, Me – methyl, TFM – trifluoromethoxy, OMe – methoxy, ED – ethyl amide, HED – hydroxyethyl amide, AED – aminoethyl amide, HD – hydrazide, HA – hydroxamic acid, CA – carboxylic acid, ME – methyl ester.

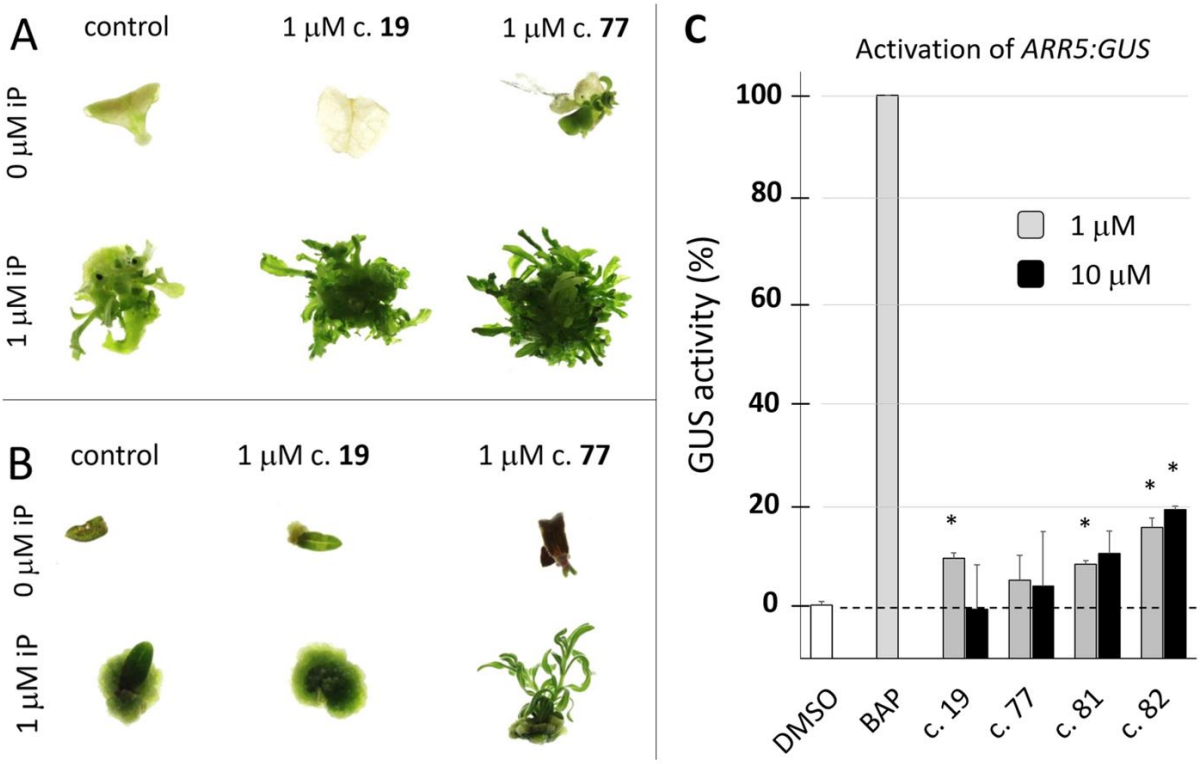

Fig. 4. Biological activity of tested compounds in different plant species. Effect of combinations of N^6-isopentenyladenine (iP) and compounds **19** and **77** on adventitious shoot regeneration of *Lobelia* (A) and *Lavandula* (B). The experiments were performed once with 20 explants for each treatment and the presented pictures are representative examples. (C) Effect of selected compounds on activation of *ARR5:GUS* in transgenic Arabidopsis plants (*ARR5* is a cytokinin primary response gene). BAP (N^6-benzylaminopurine) was used as a standard (positive control) and 0.1% DMSO as a blank control (set as 0%, dashed line). The means are relative to the activity of BAP, which was set as 100%. Error bars show the SD of the mean of two independent experiments, each performed in triplicate. Asterisks indicate statistically significant differences identified by the two-tailed Student's t-test at $P < 0.05$. The exact values are in Table S2.

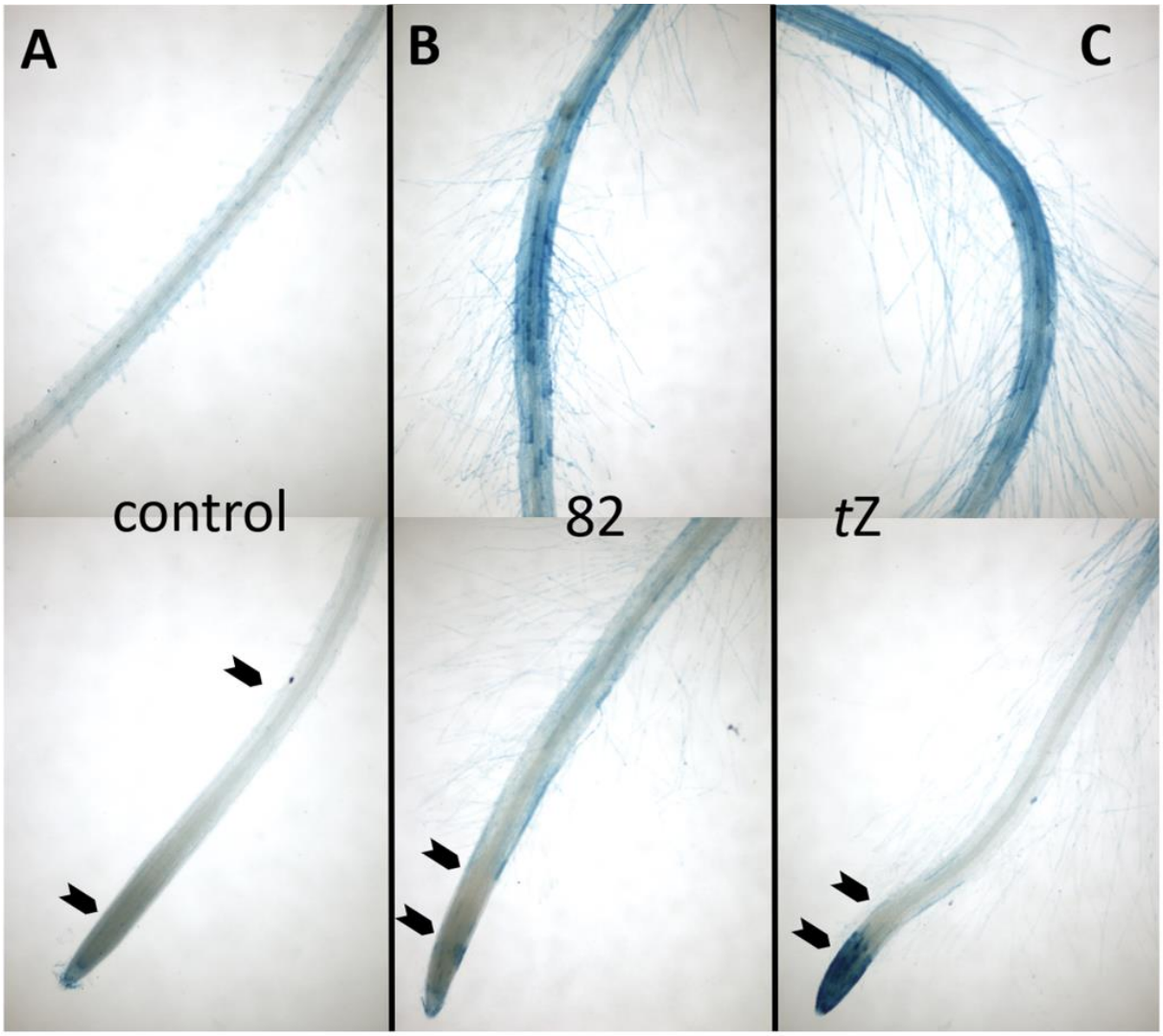

Figure 5. The effect of compound **82** and *trans*-zeatin on GUS activity in the part of the root of 8-days-old Arabidopsis seedlings with *TCSv2:uidaA (TWO-COMPONENT OUTPUT SENSOR VERSION2)* reporter gene. Plants were cultivated in the presence of 0.01% DMSO (control) (A), 1 μM compound **82** (B) or 1 μM trans-zeatin (C) in a growth medium. The upper pictures show the root with root hairs above the root tip, and the bottom pictures show the root tip divided into the maturation, elongation, and meristematic zones, respectively. Pictures of the whole seedlings are in Fig. S4.

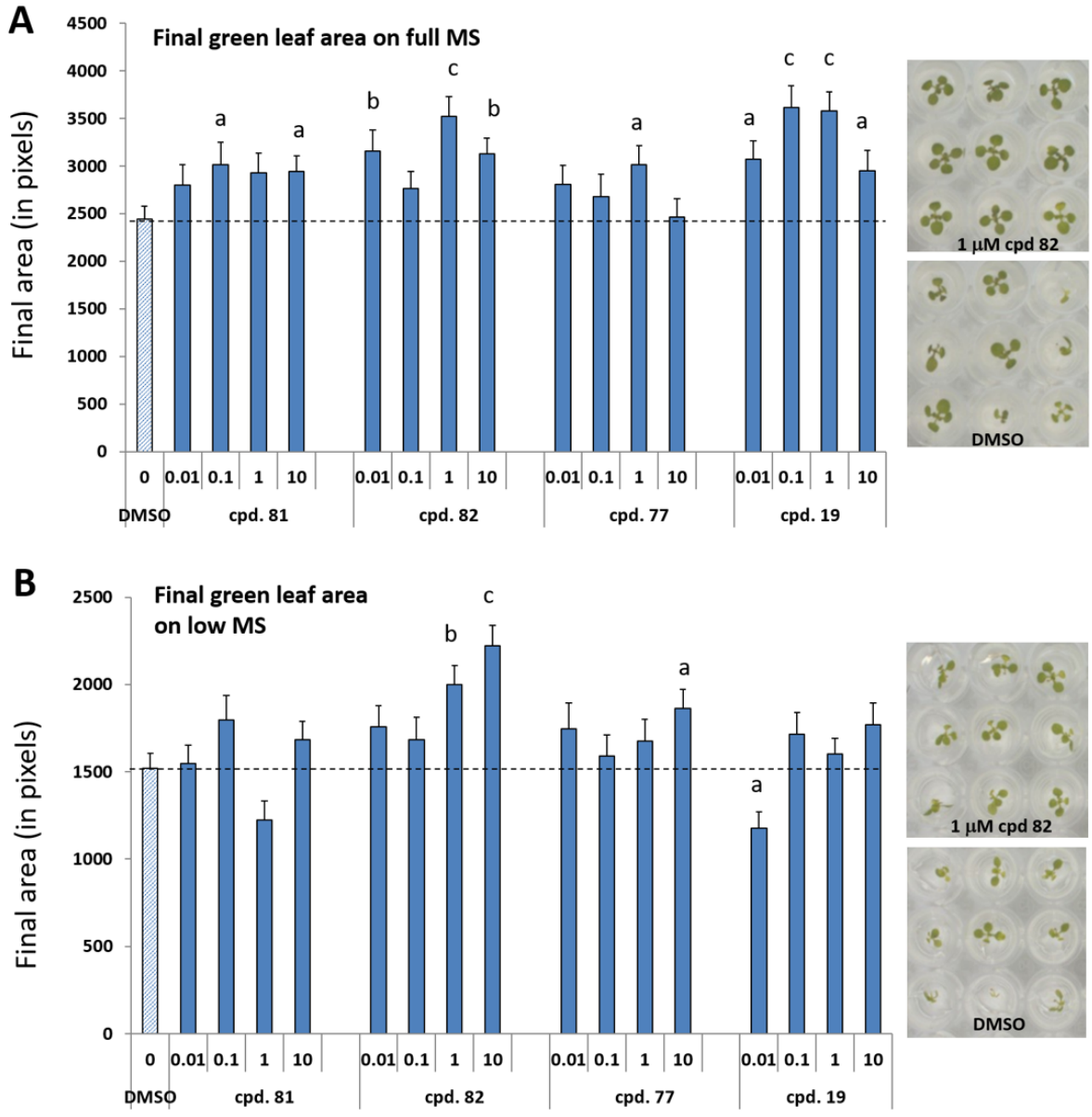

Figure 6. The effect of selected compounds on the final green leaf area of 11-day-old Arabidopsis seedlings on full (A) and low (B) MS. Compounds were tested in 0.01, 0.1, 1 and 10 µM concentrations as indicated. DMSO (0.1%) was used as solvent control (dashed line). The error bars show the SE of the mean (n = 48) from one experiment. Statistically significant differences between control (DMSO) and treatments identified by the two-tailed Student's t-test are indicated by the letters *a*, *b*, or *c*, corresponding to *P*-values of $0.05 > P > 0.01$, $0.01 > P > 0.001$, and $P < 0.001$, respectively. The inserts show that compound **82** increases shoot growth and the homogeneity of the seedling population. Pictures of the whole plates are in Fig. S5. Detailed analysis of the other plant characteristics is in Fig. S5. MS – Murashige and Skoog medium.

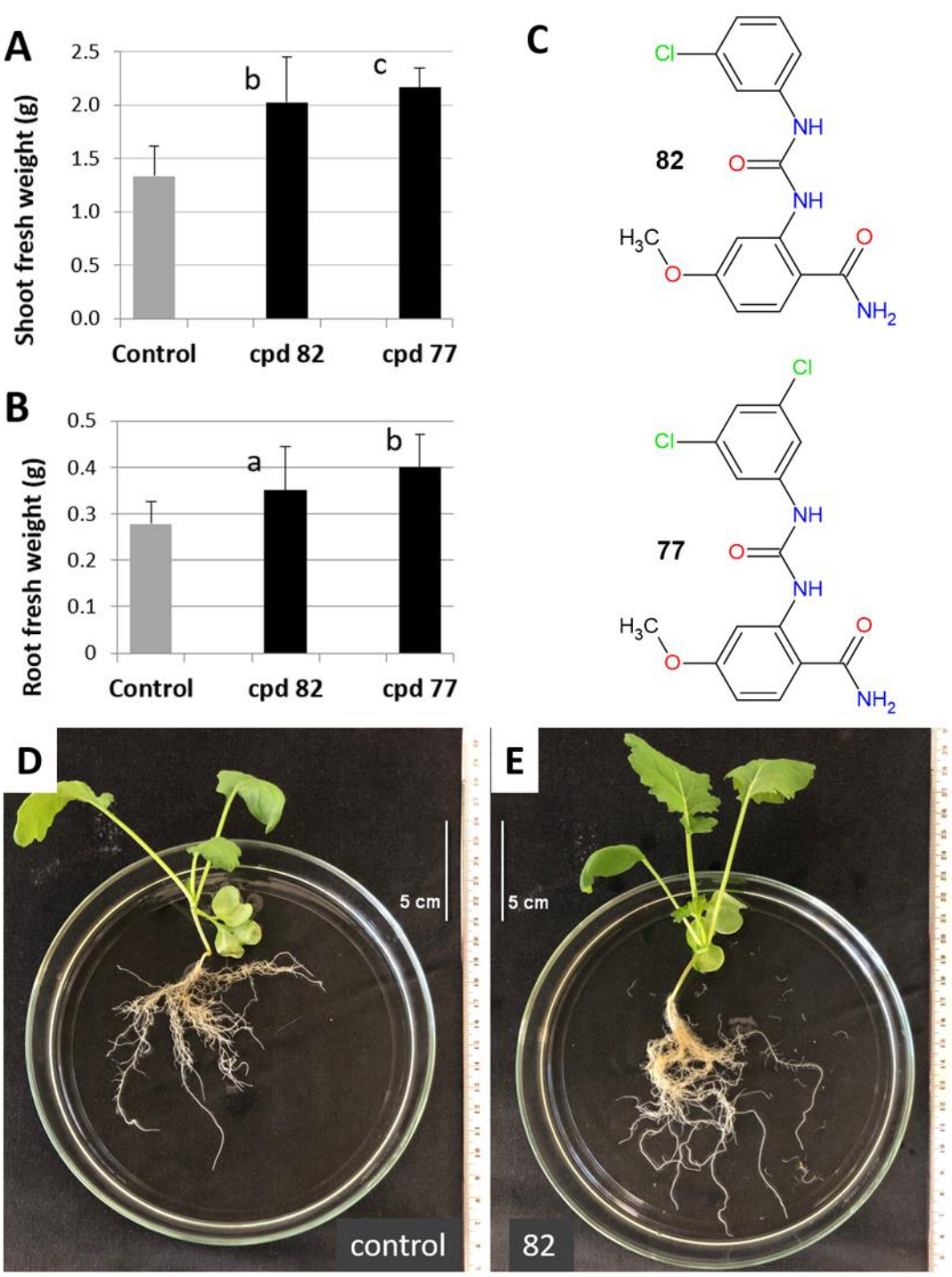

Fig. 7. Effect of compounds **77** and **82** on the growth of winter oilseed rape. (A) Shoot fresh weight. (B) Root fresh weight. (C) Structures of compounds **77** and **82**. (D, E) Photograph of average control plant (D) and average plant treated with 100 nM compound **82** (E). The plants were 22 days old. In (A, B) Statistically significant differences between means of control and treatments (n = 12 ± SD) identified by the two-tailed Student's t-test are indicated by the letters *a*, *b*, or *c*, corresponding to *P*-values of $0.05 > P > 0.01$, $0.01 > P > 0.001$, and $P < 0.001$, respectively. The entire experiment was performed one time.